Review

International Journal of Modern Physics E
Vol. 24, No. 10 (2015) 1530010 (57 pages)
© World Scientific Publishing Company
DOI: 10.1142/S0218301315300106

World Scientific
www.worldscientific.com

Introduction to hydrodynamics*

Sangyong Jeon* and Ulrich Heinz†

*Department of Physics,
McGill University, Montreal, QC, Canada

†Department of Physics,
The Ohio State University, Columbus, Ohio, USA

Received 21 July 2015
Accepted 25 July 2015
Published

Hydrodynamics has been successful in providing a good description of the bulk dynamics in ultra-relativistic heavy ion collisions. In this brief review, we provide basics of the theory of viscous hydrodynamics. Topics covered include derivation of the 2nd order viscous hydrodynamics from the linear response theory and kinetic theory, viscous anisotropic hydrodynamics, and numerical implementation of relativistic hydrodynamics.

Keywords: Relativistic heavy-ion collisions; quark-gluon plasma; viscous hydrodynamics; kinetic theory; numerical methods.

PACS Number(s): 25.75.−q, 12.38.Mh, 05.20.Dd, 24.10.Nz

1. Introduction

Application of hydrodynamics in high-energy physics has a long and illustrious history starting from L. D. Landau's seminal paper.[1] In its history of more than half a century, many papers have been written on a broad spectrum of topics, too numerous to list them all here. In this review, our emphasis will be more on the basics of the theory of hydrodynamics than to report on the current phenomenological status, of which several excellent reviews already exist (for instance, see Refs. 2–4).

Recent ultra-relativistic heavy ion collision experiments at the Super Proton Synchrotron (SPS), Relativistic Heavy Ion Collider (RHIC) and the Large Hadron Collider (LHC) have demonstrated beyond any doubt that Quark–Gluon Plasma (QGP) is being created in these collisions. Unfortunately, direct access to the QGP properties such as the temperature, equation of state, transport coefficients, etc. is not very feasible. The only experimentally accessible information is contained in the spectra of the final state particles. To connect them to the QGP properties such as

*This article will also appear in "Quark–Gluon Plasma 5" edited by X. N. Wang (World Scientific, 2016).

above, one must use theoretical models. It would be wonderful to have an analytic or a numerical method that can calculate evolution of heavy ion collisions from first principles. But this microscopic, non-equilibrium, many-body QCD problem is currently intractable. What is tractable is the coarse-grained collective motion of the system as a fluid after the local thermal equilibrium is established. Since the properties of QGP we are after are mostly (local) equilibrium properties, it is natural that the dynamics of collective motion — hydrodynamics — is an integral part of the theoretical modelling.

What has been exciting and interesting in QGP research is the close discourse between the experiment and theory. In elementary particle experiments, perturbative QCD is being tested with amazing successes. More and more precise perturbative QCD calculations prove to describe experimental data more and more accurately. In contrast, QGP research is much more dynamic. For instance, before the discovery of QGP, theoretical expectation was that QGP would be a weakly coupled plasma of quarks and gluons based partially on the fact that the QGP properties seem to approach about 80% of the Stefan–Boltzmann limit rather quickly on lattice, around $2T_c$.[5] But almost from the day-1 of RHIC operation, strong elliptic flow quickly proved this initial expectation not very viable. QGP around the transition temperature turned out to be *the* most strongly coupled many-body system ever observed. Soon after, the authors of Ref. 6 used string theory techniques to calculate the infinite coupling limit of the shear viscosity and came up with a surprising result that the limit is small, but has a non-zero lower bound. Subsequent Hydrodynamic calculations then demonstrated the importance of small but finite shear viscosity in understanding the RHIC flow data.[7–9] Comparing the ensuing LHC predictions with the LHC data now confirmed the expectation that as the temperature increases, shear viscosity of QGP should also increase.[10–13]

All these connections between exciting theoretical developments and experiments cannot be made without hydrodynamics. More recently, the systems created in the highest multiplicity proton–proton collisions and proton–nucleus collisions were also seen to exhibit strong collective behavior.[14–17] This is deeply puzzling as the size of the system ought to be too small to behave collectively. It is hoped that more thorough investigation of the possible origin of the collectivity in such small systems can illuminate the inner workings of the QGP formation greatly.[18]

As mentioned in the beginning, the aim of this review is the introduction of the theory of the hydrodynamics in ultra-relativistic heavy ion collisions. This actually entails a large number of disciplines in addition to the relativistic fluid dynamics. Our plan for this review is as follows. Section 2 contains the basic concepts of hydrodynamics and their definitions. In Sec. 3, second-order viscous hydrodynamics is derived from a very general linearly response theory of conserved currents. Section 4 discusses how coarse-graining of kinetic theory can result in more general form of viscous hydrodynamics. In Sec. 5, various numerical techniques needed to implement relativistic viscous hydrodynamics in ultra-relativistic heavy ion collisions are discussed. We conclude in Sec. 6.

2. Hydrodynamic Form of the Stress–Energy Tensor and the Net Baryon Number Current

Hydrodynamics is all about flow of conserved quantities. In this review, we strictly deal with relativistic hydrodynamics. Therefore, unlike the non-relativistic case, mass is a part of the energy budget. In the Minkowski coordinates, conservation laws in their local form are

$$\begin{aligned} \partial_\mu T^{\mu\nu} &= 0, \\ \partial_\mu J_i^\mu &= 0, \end{aligned} \tag{1}$$

where $T^{\mu\nu}$ is the stress–energy tensor and the roman letter i on the current J_i^μ labels any other conserved charges such as the net baryon number, net electric charge, etc. For the bulk evolution in relativistic heavy ion collisions, usually only the net baryon number current, J_B^μ, is considered. If needed, additional electric current and the strangeness current can be easily accommodated.

Using the divergence theorem, the integral form of the conservation laws read

$$\begin{aligned} \frac{d}{dt}\int_V d^3x\, T^{0\nu} &= -\int_{\partial V} dS_i T^{i\nu}, \\ \frac{d}{dt}\int_V d^3x\, J_B^0 &= -\int_{\partial V} dS_i J_B^i, \end{aligned} \tag{2}$$

where on the right-hand side the integration is over the boundary of the volume V assuming that the size and the shape of the volume is independent of time.

This form admits a very physical interpretation that the rate of change of the conserved quantity in a fixed volume equals the net current entering the volume. Hence, the dynamics of conserved quantities are governed by the dynamics that governs the currents. In essence, hydrodynamics is all about the dynamics of the currents.

Hydrodynamics is useful because it is a coarse-grained theory. When a system contains too many particles, it becomes difficult to follow microscopic details of the system. When the system contains sufficiently many particles, the system again starts to admit analytic studies because thermodynamic concepts start to apply, in particular the static equilibrium. A system in static equilibrium is characterized by only few quantities such as the temperature, collective velocity and chemical potential. These control the energy density, momentum density and charge density, respectively. The price to pay for this simplification is that questions on short time scale phenomena or short length scale phenomena cannot be answered any longer.

The systems we would like to study, the ultra-relativistic heavy ion collisions, do contain a large number of particles, but they certainly are not static. In fact, they will never actually reach the state of static equilibrium. Nevertheless, if one is interested only in the coarse-grained collective motion of the system, the concept

of *local equilibrium* may still apply provided that the expansion rate is much slower than the microscopic interaction rate. If one considers a macroscopically small but microscopically large fluid cell around a position $\mathbf{x}$ at a given time t, then within a macroscopically short but microscopically long time scale, the time averages should approach the static equilibrium values according to the ergodicity hypothesis of statistical mechanics. More details on the length and the time scale analysis can be found in Sec. 4.1.

When the local equilibrium is reached, it becomes meaningful to describe the system with the local temperature $T(t, \mathbf{x})$, the collective velocity $u^\mu(t, \mathbf{x})$ of the fluid cell and the local chemical potential $\mu_B(t, \mathbf{x})$. One can then study dynamics of only those few thermodynamic quantities. Since T, u^μ, μ_B are basically the Lagrange multipliers to fix the average energy, momentum and net charge, it is natural that we turn to the conservation laws for their dynamics. The goal of hydrodynamics is then to study collective motion of a system using the conservation laws with only the *statistical* inputs from the underlying microscopic theory.

In an dynamically evolving fluid, the concept of the local rest frame is essential in order to apply the concept of local equilibrium. However defining the collective velocity of a fluid cell turned out to be quite intricate. This is not so simple even for the simplest system composed of a single kind of non-interacting particles in the non-relativistic setting. One kind of collective velocity comes from the average momentum

$$\mathbf{u}_p = \frac{\sum\limits_i m\mathbf{v}_i}{\sum\limits_i m} \tag{3}$$

or from the mass current. Here the sum is over all particles in the given fluid cell. Another comes from the energy–weighted average

$$\mathbf{u}_E = \frac{\sum\limits_i (m\mathbf{v}_i^2/2)\mathbf{v}_i}{\sum\limits_i (m\mathbf{v}_i^2/2)} \tag{4}$$

or from the energy current. If the particles in the system have an additional conserved charge, B, and the net charge is non-zero, then one can define yet another collective velocity by performing the charge-weighted average

$$\mathbf{u}_B = \frac{\sum\limits_i B_i\mathbf{v}_i}{\sum\limits_i B_i}. \tag{5}$$

Here B_i is the conserved charge of the ith particle.

For a state in static equilibrium, all three collective velocities above coincide because they must all vanish. However, they do not necessarily coincide to an

observer moving with a uniform speed $-\mathbf{u}_O$. The mass weighted average velocity and the charge weighted average velocity are both $\mathbf{u}_O$. But the energy weighted average velocity

$$\mathbf{u}'_E = \frac{\sum_i (m(\mathbf{v}_i + \mathbf{u}_O)^2/2)(\mathbf{v}_i + \mathbf{u}_O)}{\sum_i m(\mathbf{v}_i + \mathbf{u}_O)^2/2} \neq \mathbf{u}_O \tag{6}$$

clearly does not coincide with $\mathbf{u}_O$. There is no unambiguous choice of the flow velocity even in this simple case. One must choose among these options what will be regarded as the flow velocity.

In the relativistic setting, mass is a part of the energy. Hence, there are only two options for choosing the flow velocity: The energy current or the net baryon current. One must choose one of these velocity options in order to decompose $T^{\mu\nu}$ and J^μ_B into a useful hydrodynamic form. The net baryon number is relatively small in ultra-relativistic heavy ion collisions. Furthermore, the flow observables we are interested in are mostly patterns in energy and momentum distributions. Therefore, there is no real benefit to choose the net baryon number collective velocity as long as the heavy ion analysis is concerned.

Choosing to follow the energy current,[a] the flow velocity for the energy current is defined by the eigenvalue problem

$$T^\mu_\nu u^\nu = \varepsilon u^\mu \tag{7}$$

where $T^\mu_\nu = T^{\mu\alpha} g_{\alpha\nu}$ and the flow vector is normalized to $u^\mu u_\mu = g_{\mu\nu} u^\mu u^\nu = 1$. We use $g_{\mu\nu} = \mathrm{diag}(1, -1, -1, -1)$ throughout this review. Note that while $T^{\mu\nu}$ is a symmetric matrix, T^μ_ν is no longer a symmetric matrix. Therefore, there is no guarantee that the eigenvalues are real. But any physically consistent system should admit a positive eigenvalue ε and the associated time-like real eigenvector u^μ.

Decomposing $T^{\mu\nu}$ using ε and u^μ, one gets

$$T^{\mu\nu} = \varepsilon u^\mu u^\nu + \frac{1}{3}(T^\alpha_\alpha - \varepsilon)\Delta^{\mu\nu} + \pi^{\mu\nu} \tag{8}$$

where the local 3-metric $\Delta^{\mu\nu}$ is given by

$$\Delta^{\mu\nu} = g^{\mu\nu} - u^\mu u^\nu. \tag{9}$$

The residual shear tensor $\pi^{\mu\nu}$ is symmetric $\pi^{\mu\nu} = \pi^{\nu\mu}$, transverse $\pi^{\mu\nu} u_\nu = 0$ and traceless $\pi^{\mu\nu} g_{\mu\nu} = 0$. Hence altogether the expression (8) has the required 10 independent degrees of freedom; the local energy density ε, the local fluid velocity

[a]This choice of frame is often referred to as the Landau–Lifshitz frame. If one choose to follow the charge current, it is referred to as the Eckart frame.

u, the trace T^α_α and the residual shear tensor $\pi^{\mu\nu}$. The net baryon current is

$$J^\mu_B = J^\mu_{B,\mathrm{id}} + V^\mu_B \tag{10}$$

where $J^\mu_{B,\mathrm{id}} = \rho_B u^\mu$ is the ideal fluid part of the current and V^μ_B is a space-like vector satisfying the transversality condition $u_\mu V^\mu_B = 0$. It has the required 4 independent degrees of freedom; the local net baryon density ρ_B and the residual vector $\mathbf{V}_B$.

So far we did not use any thermodynamic information. We will do so now to re-write the trace T^α_α in a more physical form. A static medium at rest has $T^{\mu\nu}_{\mathrm{eq}} = \mathrm{diag}(\varepsilon, P, P, P)$ where P is the pressure. Therefore, the trace should contain the equilibrium piece $g_{\mu\nu}T^{\mu\nu}_{\mathrm{eq}} = \varepsilon - 3P$. Furthermore, the thermodynamic identities

$$dP = sdT + \rho_B d\mu_B, \tag{11}$$

$$ds = \frac{1}{T}d\varepsilon - \frac{\mu_B}{T}d\rho_B, \tag{12}$$

where s is the entropy density, indicate that the pressure P is a function of the temperature T and the baryon chemical potential μ_B, and they are in turn function of the energy density and the net baryon density. Hence we must be able to find P as a function of ε and ρ_B:

$$P = P(\varepsilon, \rho_B). \tag{13}$$

This relationship is known as the equation of state. Writing $T^\alpha_\alpha = \varepsilon - 3(P + \Pi)$, the stress–energy tensor then becomes

$$T^{\mu\nu} = T^{\mu\nu}_{\mathrm{id}} - \Pi\Delta^{\mu\nu} + \pi^{\mu\nu}. \tag{14}$$

where $T^{\mu\nu}_{\mathrm{id}} = \varepsilon u^\mu u^\nu - P(\varepsilon, \rho_B)\Delta^{\mu\nu}$ is the ideal fluid stress–energy tensor.

From the arguments presented above, it should be clear that the residual scalar term Π and the tensor term $\pi^{\mu\nu}$ as well as the vector V^μ_B in the baryon current must vanish in the static equilibrium limit. As these quantities represent deviation from equilibrium, the size of these terms will depend on how fast the local equilibrium is achieved. If local equilibration is instantaneous in the macroscopic time scale, then fluid cells will always be in strict local equilibrium and hence $\Pi = \pi^{\mu\nu} = V^\mu_B = 0$. Microscopically, this would happen if scattering cross-section is large so that the mean free path is much shorter than any macroscopic time scale or length scale (c.f. Sec. 4.1). If this is the case, the number of unknowns $(\varepsilon, \mathbf{u}, \rho_B)$ matches the 5 conservation laws and one has the ideal hydrodynamics whose dynamics is completely specified by

$$\partial_\mu(\varepsilon u^\mu u^\nu - P(\varepsilon, \rho_B)\Delta^{\mu\nu}) = 0 \tag{15}$$

and

$$\partial_\mu(\rho_B u^\mu) = 0. \tag{16}$$

The information on the underlying system is only in the equation of state $P(\varepsilon, \rho_B)$.

3. Hydrodynamics from Linear Response Theory

3.1. *Linear response theory*

In realistic systems, the approach to the local equilibrium is never going to be infinitely fast. Therefore, Π, $\pi^{\mu\nu}$ and V_B^μ cannot simply be set to vanish, although if the system is conformal one strictly has $\Pi = 0$. This is because the trace must vanish $T^\alpha_\alpha = 0$ in a conformal system. When any of these quantities are non-zero, the system is out of equilibrium. Therefore, local entropy must increase. The evolution equations of these quantities are then necessarily of the dissipative type. In this and following sections, we use linear response theory to obtain such equations for dissipative hydrodynamics. In Sec. 4, kinetic theory approaches that can go beyond the near-equilibrium restriction of the linear response theory is discussed.

To gain more insights on the behavior of the dissipative quantities, we start with a system very slightly out of equilibrium at $t = 0$. We then consider how the system approaches the equilibrium. This is the realm of the linear response theory. Full analysis of the quantum linear response theory can be found in any number of standard text books (for example, see Ref. 19). Here we will only go over the main ideas.

Suppose that at the remote past, $t = -T$, the density operator had the equilibrium form $\hat{\rho}_0 = e^{-\beta\hat{H}_0}/Z_0$ where $\hat{H}_0$ is the system Hamiltonian and $Z_0 = \mathrm{Tr}e^{-\beta\hat{H}_0}$ is the partition function. Then a force term is adiabatically turned on $f(t,x) = \theta(-t)f(x)e^{\epsilon t}$ at an infinitesimally slow rate ϵ. At $t = 0$, the force term is turned off and at this point the system is out of equilibrium. The full time-dependent Hamiltonian for this process is

$$\hat{H}(t) = \hat{H}_0 - \int d^3x\, \hat{A}(x) f(t,\mathbf{x}). \tag{17}$$

Here $\hat{A}$ represents a set of Hermitian operators for the conserved quantities we are interested in. Namely, $T^{0\mu}$ and ρ_B. Hence, the expressions presented below are in general matrix expressions.

Treating $\delta\hat{H} = -\int d^3x f(t,\mathbf{x})\hat{A}(\mathbf{x})$ as a perturbation, the formal first-order solution of the quantum Liouville equation $i\partial_t\hat{\rho}(t) = [\hat{H}(t), \hat{\rho}(t)]$ is given by

$$\delta\hat{\rho}_H(t) = -i\int_{-T}^{t} dt' [\delta\hat{H}_H(t'), \hat{\rho}_0(0)] \tag{18}$$

where $\delta\hat{\rho}(t) = \hat{\rho}(t) - \hat{\rho}_0$ and the subscript H denotes Heisenberg picture operators

$$\hat{O}_H(t) = e^{i\hat{H}_0 t}\hat{O}e^{-i\hat{H}_0 t}. \tag{19}$$

Using $\delta\hat{H}$ from Eq. (17), the deviation of an observable A from the equilibrium value is found to be

$$\delta\langle\hat{A}(t,\mathbf{x})\rangle = \int d^4x'\, G_R^{AA}(t-t', \mathbf{x}-\mathbf{x}')\theta(-t')e^{\epsilon t'} f(\mathbf{x}') \tag{20}$$

where $t > 0$ and

$$G_R^{AA}(t-t', \mathbf{x}-\mathbf{x}') = i\theta(t-t')\mathrm{Tr}(\hat{\rho}_0[\hat{A}_H(t,\mathbf{x}), \hat{A}_H(t',\mathbf{x}')]) \tag{21}$$

is the retarded response function. We also took the $-T \to -\infty$ limit.

Suppose that one can find an operator $\hat{D}_A$ for which G_R^{AA} is the generalized retarded Green function,

$$\hat{D}_A G_R^{AA}(t-t', \mathbf{x}-\mathbf{x}') = \hat{d}_A \delta(t-t')\delta(\mathbf{x}-\mathbf{x}'), \tag{22}$$

where $\hat{d}_A$ can contain a finite number of derivatives. For $t > 0$, t and t' can never be the same in Eq. (20). Hence $\delta\langle\hat{A}\rangle$ satisfies the evolution equation

$$\hat{D}_A \delta\langle\hat{A}(t,\mathbf{x})\rangle = 0 \tag{23}$$

for $t > 0$. Therefore finding the pole structure of the response function is equivalent to finding the evolution equation.[20,21] We will use this to find hydrodynamic equations in the following sections.

For further analysis, it is useful to define the spectral density

$$\rho^{AA}(\omega,\mathbf{k}) = \int d^4x\, e^{i\omega t - i\mathbf{k}\cdot\mathbf{x}} \langle[\hat{A}_H(t,\mathbf{x}), \hat{A}_H^\dagger(0)]\rangle. \tag{24}$$

Using the thermal average $\langle(\cdots)\rangle = \mathrm{Tr}\hat{\rho}_0(\cdots)$, it is not hard to show (for instance, see Ref. 19)

$$\rho^{AA}(\omega,\mathbf{k}) = \frac{1}{Z_0}\sum_{m,n}(e^{-\beta E_n} - e^{-\beta E_m})(2\pi)^4\delta(k - p_m + p_n)|\langle n|\hat{A}|m\rangle|^2 \tag{25}$$

where $k = (\omega,\mathbf{k})$ and $|m\rangle$ is the simultaneous eigenstate of the system Hamiltonian $\hat{H}_0$ and the total momentum $\hat{\mathbf{P}}$ of the system with the eigenvalue $p_m = (E_m, \mathbf{p}_m)$. From this expression, we can derive

$$\rho^{AA}(-\omega,-\mathbf{k}) = -\rho^{AA}(\omega,\mathbf{k}) \tag{26}$$

by exchanging m and n. When the underlying equilibrium system is isotropic, then $\rho^{AA}(\omega,\mathbf{k})$ must be a function of $|\mathbf{k}|$ only. Hence the spectral density is an odd function of ω, $\rho^{AA}(-\omega,\mathbf{k}) = -\rho^{AA}(\omega,\mathbf{k})$. We will use this property often in later sections to parametrize the analytic structure of the response functions.

In terms of ρ^{AA}, the retarded correlator is

$$G_R^{AA}(\omega,\mathbf{k}) = \int \frac{d\omega'}{2\pi}\frac{\rho^{AA}(\omega',\mathbf{k})}{\omega'-\omega-i\epsilon}. \tag{27}$$

The imaginary part of the retarded correlator directly gives the spectral density

$$\mathrm{Im}\, G_R^{AA}(\omega,\mathbf{k}) = \frac{1}{2}\rho^{AA}(\omega,\mathbf{k}). \tag{28}$$

It is also useful to know that the Euclidean correlator is given by (for derivations, see, for instance, Ref. 19)

$$G_E^{AA}(\omega_n,\mathbf{k}) = \int \frac{d\omega'}{2\pi}\frac{\rho^{AA}(\omega',\mathbf{q})}{\omega'-i\omega_n} \tag{29}$$

where $\omega_n = 2\pi nT$ is the Matsubara frequency. One important fact we will often use in the following sections is that the $\omega \to 0$ limit

$$G_R^{AA}(0,\mathbf{k}) = G_E^{AA}(0,\mathbf{k}) = \int \frac{d\omega'}{2\pi} \frac{\rho^{AA}(\omega,\mathbf{k})}{\omega'}$$
$$= \frac{1}{Z_0}\sum_{m,n}(e^{-\beta E_n} - e^{-\beta E_m})$$
$$\times \frac{1}{E_m - E_n}(2\pi)^3\delta(\mathbf{k} - \mathbf{p}_m + \mathbf{p}_n)|\langle n|\hat{A}|m\rangle|^2 \qquad (30)$$

is real and positive and function only of the magnitude of $\mathbf{k}$.[b]

3.2. *Baryon density diffusion*

From the previous section, it is clear that the analytic structure of the response function determines the evolution of small disturbances. In this and the following sections, we show that this fact combined with the conservation laws is powerful enough to produce dissipative hydrodynamic equations.

The analysis in this section and those up to Sec. 3.5 closely follow the unpublished note by Laurence G. Yaffe (private communication, see also Refs. 22 and 23) in a simplified form. Additional discussion on the second-order formulation of dissipative hydrodynamics is given in Sec. 3.6.

We start with the net baryon number conservation which is the simplest to examine. Suppose we set up a system where only the net baryon density $\langle\rho_B(0,\mathbf{x})\rangle$ is non-uniform at $t = 0$. The perturbing Hamiltonian is

$$\delta\hat{H}(t) = -\int d^3x\, \hat{\rho}_B(\mathbf{x})\, e^{\epsilon t}\mu_B(\mathbf{x}) \qquad (31)$$

which results in the following linear response in the mixed space of t and the wave vector $\mathbf{k}$,

$$\delta\langle\hat{\rho}_B(t,\mathbf{k})\rangle = \mu_B(\mathbf{k})\int_{-\infty}^{\infty} dt'\,\theta(-t')e^{\epsilon t'}G_R^{00}(t-t',\mathbf{k}) \qquad (32)$$

for $t > 0$.

Applying the current conservation, $\partial_t\rho_B = -\nabla\cdot\mathbf{J}_B$, to the retarded correlation functions $G_R^{\mu\nu}(t,\mathbf{x}) = i\theta(t)\langle[\hat{J}_B^\mu(t,\mathbf{x}), \hat{J}_B^\nu(0)]\rangle$ results in the following relationships between them in the frequency–wave vector space

$$\omega G_R^{00}(\omega,\mathbf{k}) = k_i G_R^{0i}(\omega,\mathbf{k}), \qquad (33)$$

$$\omega G_R^{0j}(\omega,\mathbf{k}) = k_i G_R^{ij}(\omega,\mathbf{k}) \qquad (34)$$

provided that $[J_B^0(0,\mathbf{x}), J_B^\nu(0,\mathbf{x}')] = 0$. The underlying isotropic equilibrium permits decomposition into transverse and the longitudinal parts

$$G_R^{ij}(\omega,\mathbf{k}) = \hat{k}^i\hat{k}^j G_L(\omega,\mathbf{k}^2) + \hat{\delta}^{ij}G_T(\omega,\mathbf{k}) \qquad (35)$$

[b]To see this, just exchange m and n.

where $\hat{\mathbf{k}} = \mathbf{k}/|\mathbf{k}|$ is the unit vector and $\hat{\delta}^{ij} = \delta^{ij} - \hat{k}^i\hat{k}^j$ is the transverse projector. Combining Eqs. (33) and (34) gives

$$\omega^2 G_R^{00}(\omega, \mathbf{k}) = \mathbf{k}^2 G_L(\omega, \mathbf{k}). \tag{36}$$

What we are interested in is the behavior of $G_L(\omega, \mathbf{k})$.

Consider the small ω limit of G_L first. From Eq. (30), we know that

$$g_{00}(\mathbf{k}) = G_R^{00}(0, \mathbf{k}) = G_E^{00}(0, \mathbf{k}) \tag{37}$$

is real and positive. The small ω limit of G_L can be then expressed as

$$G_L(\omega, \mathbf{k}) \approx \frac{\omega^2 g_{00}(\mathbf{k})}{\mathbf{k}^2}. \tag{38}$$

Now consider taking the $\mathbf{k} \to 0$ limit with a fixed $\omega \neq 0$. The retarded density–density correlation function in this limit is

$$\begin{aligned} G_R^{00}(\omega, 0) &= i\int_0^\infty dt\, e^{-i\omega t} \int d^3x \langle[\hat{\rho}_B(t, \mathbf{x}), \hat{\rho}_B(0)]\rangle \\ &= i\int_0^\infty dt\, e^{-i\omega t} \langle[\hat{Q}_B, \hat{\rho}_B(0)]\rangle = 0 \end{aligned} \tag{39}$$

where we used the fact that $\hat{Q}_B = \int d^3x\, \hat{\rho}_B(t, \mathbf{x})$ is the net baryon number operator. Since the net baryon number is conserved, $\hat{Q}_B$ is independent of time. In particular, it can be evaluated at $t = 0$. Therefore, the commutator vanishes. This then indicates that $G_L(\omega, \mathbf{k})$ is well behaved in the zero $|\mathbf{k}|$ limit with $\omega \neq 0$. Consequently, the $\omega \to 0$ limit and the $\mathbf{k} \to 0$ limit do not commute, indicating the presence of a massless pole. We also know that the imaginary part of G_R^{00} (the spectral density ρ^{00}) has to be an odd function of ω since isotropy in space demands that it be a function only of $\mathbf{k}^2$ (c.f. Eq. (26)).

The most general form of G_L consistent with the above conditions is

$$G_L(\omega, \mathbf{k}) = \frac{\omega^2(g_{00}(\mathbf{k}) + i\omega A(\omega, \mathbf{k}))}{\mathbf{k}^2 - i\omega/D(\omega, \mathbf{k}) - \omega^2 B(\omega, \mathbf{k})}. \tag{40}$$

The functions $D(\omega, \mathbf{k})$, $A(\omega, \mathbf{k})$ and $B(\omega, \mathbf{k})$ are all of the form

$$D(\omega, \mathbf{k}) = D_R(\omega, \mathbf{k}) - i\omega D_I(\omega, \mathbf{k}) \tag{41}$$

where $D_R(\omega, \mathbf{k})$ and $D_I(\omega, \mathbf{k})$ are real-valued even functions of ω and $\mathbf{k}$. The real parts D_R and B_R must have a non-zero limit as $\omega \to 0$ and $\mathbf{k} \to 0$. All other parts of A, B and D must have finite limits as $\omega \to 0$ and $\mathbf{k} \to 0$. In the small ω and $\mathbf{k}$ limit, the response function becomes

$$G_R^{00}(\omega, \mathbf{k}) \approx \frac{D\mathbf{k}^2 g_{00}(0)}{-i\omega + D\mathbf{k}^2} \tag{42}$$

where we defined the diffusion constant $D = D_R(0, 0)$.

The pole structure of G_R^{00} dictates that in the small ω and $|\mathbf{k}|$ limit, $\delta\rho_B(t,\mathbf{x}) = \delta\langle\hat{\rho}_B(t,\mathbf{x})\rangle$ obeys the diffusion equation

$$\partial_t \delta\rho_B = D\nabla^2\delta\rho_B. \tag{43}$$

This is our first example of a dissipative hydrodynamic equation. The conservation law, current algebra, thermodynamic stability, and the general analytic structure of the correlation functions are all the ingredients one needs to get this diffusion equation for baryon density. Hence diffusion is a very general phenomenon whenever there is a conserved current. Microscopic dynamics only enters through the value of the diffusion constant.

If we now go back to the conservation equation

$$\partial_t \delta\rho_B = -\partial_i \delta J_B^i, \tag{44}$$

we can see that the diffusion equation above is equivalent to the constitutive relationship

$$\delta J^i = V_B^i = D\partial^i \delta\rho_B \tag{45}$$

valid in the fluid cell rest frame. In the more general frame boosted by u^μ, it becomes

$$V_B^\mu = D\Delta^{\mu\nu}\partial_\nu\rho_B, \tag{46}$$

where again $\Delta^{\mu\nu} = g^{\mu\nu} - u^\mu u^\nu$ is the local 3-metric.

The diffusion constant can be calculated by taking the appropriate limits of G_L,

$$\lim_{\omega\to 0}\lim_{\mathbf{k}\to 0}\frac{1}{\omega}\mathrm{Im}\, G_L(\omega,\mathbf{k}) = Dg_{00}(0), \tag{47}$$

which is our first example of the Kubo formula that relates an *equilibrium* correlation function to a dissipative coefficient. As the response function is singular in the small ω and small $\mathbf{k}$ limit, the order of limits in the Kubo formula is important. The $\mathbf{k}\to 0$ limit must be taken first. Since the transport coefficients are defined as Lorentz scalars, Eq. (47) is to be evaluated using the underlying microscopic theory such as thermal QCD in the rest frame of the equilibrium system.

3.3. *Stress–energy tensor correlation functions*

To carry out the linear response analysis of the energy–momentum currents and their hydrodynamic and dissipative behavior, one need to know the Ward identity among the correlation functions. Defining the retarded correlation functions of $\hat{T}^{\mu\nu}$ turned out to be not so straightforward due to the fact that the conserved quantities $\hat{P}^\mu = \int d^3x\,\hat{T}^{0\mu}$ are also the generators of the space-time evolution. Hence, in general the equal time commutators of $\hat{T}^{0\mu}$ are non-zero unlike the net baryon current case.

To begin the analysis, consider the static partition function given by

$$Z_E[g_E] = \int \mathcal{D}\phi e^{-S_E[\phi,g_E]} \tag{48}$$

where

$$S_E[\phi, g_E] = \int d^3x \int_0^\beta d\tau \sqrt{g_E}\, \mathcal{L}(\phi, g_E) \tag{49}$$

is the Euclidean action and τ is the imaginary time. Here, ϕ denotes the collection of field variables and g_E is the Euclidean metric.

Using the Hilbert definition of the stress–energy tensor density, we have

$$\langle T^{\mu\nu}(x)\rangle_E = -2\frac{\delta}{\delta g^E_{\mu\nu}(x)} \ln Z_E[g_E]. \tag{50}$$

The two point functions are given by

$$\begin{aligned}\bar{G}^{\alpha\beta,\mu\nu}_R(x_E, y_E) &= \langle \mathcal{T}_\tau T^{\mu\nu}(x_E) T^{\alpha\beta}(y_E)\rangle_E \\ &= 4\frac{\delta^2}{\delta g^E_{\alpha\beta}(y_E)\delta g^E_{\mu\nu}(x_E)} \ln Z_E[g_E]\end{aligned} \tag{51}$$

where $x_E = (\tau, \mathbf{x})$ and $\mathcal{T}_\tau$ is the time ordering operator in τ. For the tensor density $T^{\mu\nu}$, the covariant conservation law is

$$\partial_\mu \langle T^{\mu\nu}\rangle_E + \Gamma^\nu_{\sigma\rho}\langle T^{\sigma\rho}\rangle_E = 0 \tag{52}$$

where $\Gamma^\nu_{\sigma\rho} = \frac{1}{2} g^{\mu\nu}_E (g^E_{\sigma\mu,\rho} + g^E_{\rho\mu,\sigma} - g^E_{\sigma\rho,\mu})$ is the Christoffel symbol.

By differentiating Eq. (52) once more with respect to $g^E_{\alpha\beta}(y)$, we obtain the Ward identity among the Euclidean correlation functions in the flat space,[22,23] where $g^{\mu\nu}_E = \delta^{\mu\nu}$,

$$0 = k^E_\alpha (\bar{G}^{\alpha\beta,\mu\nu}_E(k_E) + \delta^{\beta\mu}\langle T^{\alpha\nu}\rangle + \delta^{\beta\nu}\langle T^{\alpha\mu}\rangle - \delta^{\alpha\beta}\langle T^{\mu\nu}\rangle). \tag{53}$$

Here $k^\alpha_E = (\omega_n, \mathbf{k})$ and $\omega_n = 2\pi n T$ is the Matsubara frequency.

To obtain the real time correlation functions, we perform the analytic continuation. From Eqs. (27) and (29) one can see that the analytically continuation

$$\omega_n \to -ik^0 + \epsilon \tag{54}$$

changes the Euclidean correlation function to the real-time retarded correlation function. This also means that each time index of $T^{\mu\nu}$ gets a factor of $(-i)$. Since our Minkowski metric is mostly negative, going from the Euclidean metric to the mostly negative Minkowski metric means $\delta_{\mu\nu} \to -g_{\mu\nu}$. The real-time version of Eq. (53) is then

$$0 = k_\alpha (\bar{G}^{\alpha\beta,\mu\nu}_R(k) - g^{\beta\mu}\langle T^{\alpha\nu}\rangle - g^{\beta\nu}\langle T^{\alpha\mu}\rangle + g^{\alpha\beta}\langle T^{\mu\nu}\rangle) \tag{55}$$

where $k^\mu = (\omega, \mathbf{k})$.

The presence of the single stress–energy tensor average terms in Eq. (55) implies that the correlation function $\bar{G}^{\alpha\beta,\mu\nu}_R(x, x')$ is not the same as

$$G^{\mu\nu,\alpha\beta}_R(x, x') = i\theta(t)\langle[\hat{T}^{\mu\nu}(t, \mathbf{x}), \hat{T}^{\alpha\beta}(t', \mathbf{x}')]\rangle_{\rm eq}, \tag{56}$$

but differs by terms containing $\delta(x - x')$ (as well as the contact terms containing spatial derivatives of $\delta(x - x')$[24]). As the response function in the linear response

theory, these delta-function terms do not matter since t and $t' < t$ can never be the same.

Defining the real-time correlation function by the analytic continuation of the Euclidean correlation function enables us to gain the following important relationship between the two

$$\bar{G}_E^{\mu\nu,\alpha\beta}(0,\mathbf{k}) = \bar{G}_R^{\mu\nu,\alpha\beta}(0,\mathbf{k}) \tag{57}$$

which has a well-defined limit (μ and ν here are not summed)

$$\lim_{\mathbf{k}\to 0} \bar{G}_R^{\mu\nu,\mu\nu}(0,\mathbf{k}) = \lim_{\mathbf{k}\to 0} \bar{G}_E^{\mu\nu,\mu\nu}(0,\mathbf{k}) > 0. \tag{58}$$

3.4. *Momentum diffusion and shear viscosity*

In this and the following sections for the bulk viscosity, we will not consider finite net baryon density for simplicity. For analysis with finite μ_B, see Ref. 23.

Suppose that we set up a system where the flow velocity at $t = 0$ has a single non-zero component in the x-direction $u_x(y)$ which depend only on y. In this situation, two layers of the fluid at y and at $y + \Delta y$ have different fluid velocities in the orthogonal x-direction. In ideal hydrodynamics, this difference is maintained because there is no dissipation. In a normal fluid, however, particle diffusion between the two layers will eventually make them move with the same equilibrated speed. How fast two layers equilibrate depends on the size of the scattering mean free path, which in turn determines the diffusion constant, or the shear viscosity.

To set up a shear flow, let the perturbing Hamiltonian be

$$\delta\hat{H}(t) = -\int d^3x\, e^{\epsilon t}\hat{T}^{x0}(t,\mathbf{x})\beta_x(y). \tag{59}$$

The corresponding linear response is

$$\delta\langle T^{x0}(t,k_y)\rangle = \beta_x(k_y)\int_{-\infty}^{\infty} dt'\theta(-t')e^{\epsilon t'}\bar{G}_R^{x0,x0}(t-t',k_y) \tag{60}$$

for $t > 0$.

In Eq. (55), $\bar{G}_R^{x0,x0}$ appears in the following sequences when $\mathbf{k} = (0,k_y,0)$

$$\omega(\bar{G}_R^{x0,x0}(\omega,k_y) + \varepsilon) = k_y\bar{G}_R^{x0,xy}(\omega,k_y), \tag{61}$$

$$\omega\bar{G}_R^{x0,xy}(\omega,k_y) = k_y(\bar{G}_R^{xy,xy}(\omega,k_y) + P). \tag{62}$$

Combined, these become

$$\bar{G}_R^{xy,xy}(\omega,k_y) + P = \frac{\omega^2}{k_y^2}(\bar{G}_R^{x0,x0}(\omega,k_y) + \varepsilon). \tag{63}$$

Except the extra P and ε, the structure of these equations is exactly the same as the baryon current case. The following analysis is therefore a repeat of that case.

In the $\omega \to 0$ limit, $\bar{G}_R^{x0,x0}(\omega,k_y)$ must have a well defined limit since it is a thermodynamic quantity. Furthermore, the imaginary part of $\bar{G}_R^{xy,xy}(\omega,k_y)$ must

be an odd function of ω. As in the baryon current case, the $k_y \to 0$ limit of the correlation functions must be well-behaved. Thus, we can parametrize $\bar{G}_R^{xy,xy}$ as

$$\bar{G}_R^{xy,xy}(\omega, k_y) = \frac{\omega^2(\varepsilon + g_T(k_y) + i\omega A_T(\omega, k_y))}{k_y^2 - i\omega/D_T(\omega, k_y) - \omega^2 B_T(\omega, k_y)} - P \tag{64}$$

and

$$\bar{G}_R^{x0,x0}(\omega, k_y) = \frac{k_y^2(\varepsilon + g_T(k_y) + i\omega A_T(\omega, k_y))}{k_y^2 - i\omega/D_T(\omega, k_y) - \omega^2 B_T(\omega, k_y)} - \varepsilon \tag{65}$$

where $g_T(k_y) = \bar{G}_R^{x0,x0}(0, k_y)$. Here the functions A_T, B_T and D_T all have the form

$$D_T(\omega, k_y) = D_T^R(\omega, k_y) - i\omega D_T^I(\omega, k_y) \tag{66}$$

where $D_T^R(\omega, k_y)$ and $D_T^I(\omega, k_y)$ are real-valued even functions of ω and k_y. The real parts D_T^R and B_T^R must have a non-zero limit as $\omega \to 0$ and $k_y \to 0$. All other parts of A_T, B_T and D_T must have finite limits as $\omega \to 0$ and $k_y \to 0$.

In the configuration space, the constant $-\varepsilon$ term becomes $-\varepsilon\delta^4(x - x')$. In Eq. (60), this δ-function term does not contribute. Hence, in the small ω and k_y limit, the evolution of T^{x0} is determined by $i\omega = D_T k_y^2$ or

$$(\partial_t - D_T \partial_y^2) T^{x0}(t, y) = 0 \tag{67}$$

where we defined the momentum diffusion constant $D_T = D_T^R(0, 0)$. This is our second dissipative hydrodynamic equation. The diffusion equation combined with the conservation law implies the constitutive relationship

$$T^{xy}(t, y) = D_T \partial^y T^{x0}(t, y) = \eta \partial^y u^x \tag{68}$$

valid in the local rest frame. Here $\eta = D_T(\varepsilon + P)$ is the shear viscosity. It is clear from Eq. (67) that D_T has the physical interpretation of the diffusion constant for momentum diffusion.

Recognizing Eq. (68) to be a part of the spin-2 component of the second rank tensor, we can generalize this result to

$$\pi_{\rm NS}^{ij}(t, \mathbf{x}) = \eta \left(\partial^i u^j + \partial^j u^i - \frac{2g^{ij}}{3} \partial_l u^l \right) \tag{69}$$

again in the rest frame of the fluid cell. In the moving frame, this becomes

$$\pi_{\rm NS}^{\mu\nu}(t, \mathbf{x}) = 2\eta \Delta_{\alpha\beta}^{\mu\nu} \partial^\alpha u^\beta \equiv 2\eta \sigma^{\mu\nu} \tag{70}$$

where $\sigma^{\mu\nu}$ is the velocity shear tensor and $\Delta_{\alpha\beta}^{\mu\nu}$ is the spin-2 projector defined by

$$\Delta_{\alpha\beta}^{\mu\nu} = \frac{1}{2} \left(\Delta_\alpha^\mu \Delta_\beta^\nu + \Delta_\alpha^\nu \Delta_\beta^\mu - \frac{2}{3} \Delta^{\mu\nu} \Delta_{\alpha\beta} \right). \tag{71}$$

Here the label NS indicates that this is the Navier–Stokes form of the shear tensor. The Kubo formula for the shear viscosity is

$$\lim_{\omega \to 0} \lim_{k_y \to 0} \frac{1}{\omega} \mathrm{Im}\, \bar{G}_R^{xy,xy}(\omega, k_y) = D_T(\varepsilon + P) = \eta \tag{72}$$

where we used the fact that $g_T(0) = P$ which can be determined from Eq. (55).

The Kubo formula for the shear viscosity η can be also expressed in terms of the full shear-tensor correlation function[20,21]

$$\eta = \lim_{\omega\to 0}\lim_{\mathbf{k}\to 0}\frac{1}{10\omega}\mathrm{Im}\bar{G}_R^{\pi_{ij},\pi_{ij}}(\omega,\mathbf{k}) \tag{73}$$

where the shear-tensor is given by

$$\pi_{ij} = T_{ij} - (\delta_{ij}/3)T_k^k. \tag{74}$$

3.5. *Sound propagation and bulk viscosity*

So far, only the diffusion type of hydrodynamic flow is discussed which are not the main bulk excitation. To get the main excitation which must also include the ideal hydrodynamics part, one needs to look at the disturbance in the energy density. This bulk excitation, of course, is the sound wave.

Suppose we perturb the energy density with

$$\delta\hat{H}(t) = -\int d^3x e^{\epsilon t}\,\hat{T}^{00}(t,\mathbf{x})\beta_0(\mathbf{x}). \tag{75}$$

The linear response is then

$$\delta\langle T^{00}(t,\mathbf{k})\rangle = \beta_0(\mathbf{k})\int_{-\infty}^{\infty} dt'\theta(-t')e^{\epsilon t'}\bar{G}_R^{00,00}(t-t',\mathbf{k}). \tag{76}$$

Applying the conservation law to each index of $\bar{G}_R^{\mu\nu,\alpha\beta}$ in Eq. (55), we get

$$\omega^4\bar{G}_R^{00,00}(\omega,\mathbf{k}) = \omega^4\varepsilon - \omega^2\mathbf{k}^2(\varepsilon+P) + \mathbf{k}^4\bar{G}_L(\omega,\mathbf{k}) \tag{77}$$

where

$$\mathbf{k}^4\bar{G}_L(\omega,\mathbf{k}) = k_ik_jk_lk_m(\bar{G}_R^{ij,lm}(\omega,\mathbf{k}) + P(\delta^{il}\delta^{jm}+\delta^{im}\delta^{jl}-\delta^{ij}\delta^{lm})). \tag{78}$$

In the small ω limit, Eq. (77) gives

$$\bar{G}_L(\omega,\mathbf{k}) \approx \frac{\omega^2}{\mathbf{k}^2}(\varepsilon+P) + \frac{\omega^4}{\mathbf{k}^4}(\bar{G}_R^{00,00}(0,\mathbf{k}) - \varepsilon). \tag{79}$$

We also know that the imaginary part of $\bar{G}_L$ must be an odd function of ω and the correlation functions are well-behaved in the $\mathbf{k}\to 0$ limit. The most general form consistent with these conditions is

$$\bar{G}_L(\omega,\mathbf{k}) = \frac{\omega^2(\varepsilon+P+i\omega^3Q(\omega,\mathbf{k}))}{\mathbf{k}^2-\omega^2/Z(\omega,\mathbf{k})+i\omega^3R(\omega,\mathbf{k})}. \tag{80}$$

Here $Z(\omega,\mathbf{k})$, $Q(\omega,\mathbf{k})$ and $R(\omega,\mathbf{k})$ all have the form

$$Z(\omega,\mathbf{k}) = Z_R(\omega,\mathbf{k}) - i\omega Z_I(\omega,\mathbf{k}) \tag{81}$$

where $Z_R(\omega,\mathbf{k})$ and $Z_I(\omega,\mathbf{k})$ are real-valued even functions of ω and $\mathbf{k}$. The real parts Z_R and R_R must have non-zero limits as $\omega\to 0$ and $\mathbf{k}\to 0$. All other parts

of Z, Q and R must have finite limits as $\omega \to 0$ and $\mathbf{k} \to 0$. Matching the small ω limit (79) demands that

$$Z_R(0,\mathbf{k}) = \frac{\varepsilon + P}{\bar{G}_R^{00,00}(0,\mathbf{k}) - \varepsilon}. \tag{82}$$

Up to the quadratic terms in ω and $\mathbf{k}$, the poles of $\bar{G}_L(\omega,\mathbf{k})$ for small ω and $|\mathbf{k}|$ are determined by

$$\omega^2 - Z_R(0,0)\mathbf{k}^2 + i\omega Z_I(0,0)\mathbf{k}^2 = 0. \tag{83}$$

This has the structure of the dispersion relationship of a damped sound wave. Hence, in the small ω and the small $|\mathbf{k}|$ limit, $Z_R(0,0) = v_s^2$ is the speed of sound squared and $Z_I(0,0)$ is the sound damping coefficient.

To relate $Z_I(0,0)$ to the shear and the bulk viscosities, let us consider the constitutive relationships once again. From the shear part, we already have the spin-2 part of the stress tensor in the fluid cell rest frame

$$\pi^{ij}_{\rm NS}(t,\mathbf{x}) = D_T\left(\partial^i T^{j0} + \partial^j T^{i0} - \frac{2g^{ij}}{3}\partial_l T^{l0}\right). \tag{84}$$

To this we add a spin-0 part $-\gamma g^{ij}\partial_t\varepsilon = \gamma g^{ij}\partial_l T^{l0}$ to get

$$\delta T^{ij}(t,\mathbf{x}) = D_T\left(\partial^i T^{j0} + \partial^j T^{i0} - \frac{2g^{ij}}{3}\partial_l T^{l0}\right) + \gamma g^{ij}\partial_l T^{l0}. \tag{85}$$

The energy conservation law in the local rest frame[c] now becomes using Eq. (14) with the dissipative part given by Eq. (85)

$$\begin{aligned} 0 &= \partial_\mu\partial_\nu T^{\mu\nu} \\ &= \partial_t^2\varepsilon - \nabla^2 P - D_T\frac{4}{3}\nabla^2\partial_t\varepsilon - \gamma\nabla^2\partial_t\varepsilon \\ &\to (-\omega^2 + v_s^2\mathbf{k}^2 - i(4D_T/3+\gamma)\mathbf{k}^2\omega)\delta\varepsilon \end{aligned} \tag{86}$$

where we used $g^{ij}\partial_i\partial_j = -\nabla^2$ and $\partial_t\varepsilon = -\partial_l T^{l0}$. Comparing with Eq. (83), one can identify $v_s^2 = \partial P/\partial\varepsilon = Z_R(0,0)$, and

$$Z_I(0,0) = \Gamma = 4D_T/3 + \gamma \tag{87}$$

as the sound attenuation constant. Since we have already identified $D_T = \eta/(\varepsilon+P)$, this allows us to identify $\gamma = \zeta/(\varepsilon + P)$ where ζ is the bulk viscosity. In the fluid cell rest frame, the added term corresponds to the constitutive relationship $\Pi_{\rm NS} = -\zeta\partial_i u^i$. In the general frame, this becomes

$$\Pi_{\rm NS} = -\zeta\partial_\mu u^\mu. \tag{88}$$

Again, the label NS indicates that this is the Navier–Stokes form of the bulk pressure. The minus sign in Eq. (88) makes sense since the effective pressure $P + \Pi$

[c]In the local rest frame, $\mathbf{u}(t,\mathbf{x}) = 0$, but $\partial_i u_j \neq 0$.

should be less than the equilibrium pressure when the fluid is expanding (positive $\partial_i u^i$).

We have so far identified $Z_R(0,0)$ and $Z_I(0,0)$ as the speed of sound squared and the sound attenuation coefficient. The role of $R(\omega, \mathbf{k})$ is still to be identified. In the Kubo formula for the attenuation coefficient, $R_R(0,0)$ appears as

$$\lim_{\omega\to 0}\lim_{\mathbf{k}\to 0} \mathrm{Im}\,\frac{\bar{G}_L(\omega,\mathbf{k})}{\omega} = (\varepsilon + P)(Z_I(0,0) - Z_R(0,0)^2\, R_R(0,0)) \tag{89}$$

which does not allow one to identify the right-hand side with Γ if $R_R(0,0) \neq 0$. Actually, the left-hand side of Eq. (89) does yield Γ. It is just that we have not been consistent in power counting since the wave equation Eq. (86) does not contain $O(\omega^3)$ term while the pole of $\bar{G}_L$ does. One may consider this discrepancy as the first sign of the trouble with the first-order constitutive relationship Eq. (85).

3.6. *Second-order viscous hydrodynamics*

Let us consider the consequence of having the first-order constitutive relationship more closely. The diffusion equation with a source S

$$(\partial_t - D_T\nabla^2)\delta n(t,\mathbf{x}) = S(t,\mathbf{x}) \tag{90}$$

has the solution

$$\delta n(x) = \int d^4x' G_R(x-x')S(x'). \tag{91}$$

Here the retarded Green function is

$$G_R(x-x') = \theta(t-t')\frac{e^{-\frac{|\mathbf{x}-\mathbf{x}'|^2}{4D(t-t')}}}{8(\pi D(t-t'))^{3/2}}. \tag{92}$$

If one has a point source, $S(x') = N_0\delta(x')$, then $\delta n(t,\mathbf{x}) = N_0 G_R(t,\mathbf{x})$. At $t = 0$, the space is empty except at the origin. But at any time after that, there is non-zero δn everywhere. This is clearly acausal.

On the other hand, the solution of the sound equation

$$-(\partial_t^2 - v_s^2\nabla^2)\delta\epsilon(x) = S(x) \tag{93}$$

for a point source $S(x) = \Lambda_0\delta(x)$ is

$$\delta\epsilon(t,\mathbf{x}) = \Lambda_0\theta(t)\frac{1}{4\pi}\frac{\delta(|\mathbf{x}| - v_s t)}{|\mathbf{x}|}. \tag{94}$$

This is causal since the disturbance only moves with the speed of sound.

The origin of acausality in diffusion is the mismatch between the number of time derivatives and the number of spatial derivatives in the diffusion equation.

The diffusive dispersion relationship $\omega = -iD\mathbf{k}^2$ gives the group velocity

$$\frac{\partial\omega}{\partial\mathbf{k}} = -2iD\mathbf{k} \tag{95}$$

which becomes large in the large $\mathbf{k}$ limit. This problem can be remedied if one replaces the constitutive equation, $J^i = D\partial^i n$ with a relaxation type equation

$$\partial_t J^i = -\frac{1}{\tau_R}(J^i - D\partial^i n) \tag{96}$$

then the conservation law becomes

$$\begin{aligned}\partial_t^2 n &= -\partial_i\partial_t J^i \\ &= -\frac{1}{\tau_R}\partial_t n + \frac{D}{\tau_R}\nabla^2 n.\end{aligned} \tag{97}$$

For large k where we previously had a problem, we now have

$$\omega^2 \approx v_R^2 k^2 \tag{98}$$

with the propagation speed $v_R = \sqrt{D/\tau_R}$.

This type of relaxation equation was actually anticipated already: Up to the second-order in ω, the poles of the density–density correlator in Eq. (40) are determined by

$$D\mathbf{k}^2 - i\omega - \omega^2 DB = 0. \tag{99}$$

Comparing, we see that

$$B = \tau_R/D. \tag{100}$$

For the viscous stress–energy tensor components, the following relaxation equations apply in the local rest frame

$$\left(\partial_t + \frac{1}{\tau_\pi}\right)\pi^{ij} = \frac{1}{\tau_\pi}\pi^{ij}_{\rm NS}, \tag{101}$$

$$\left(\partial_t + \frac{1}{\tau_\Pi}\right)\Pi = \frac{1}{\tau_\Pi}\Pi_{\rm NS} \tag{102}$$

where

$$\pi^{lm} = T^{lm} - \frac{g^{lm}}{3}T^k_k \tag{103}$$

is the traceless part of the stress tensor and

$$\Pi = -\left(\frac{1}{3}T^k_k + P\right) \tag{104}$$

is the bulk pressure. They are not to be identified with the Navier–Stokes forms (84) and (88). Rather, they will relax to the Navier–Stokes forms.

To see if the acausality in the momentum diffusion is cured, we start with the momentum conservation

$$\partial_t T^{k0} = -\partial_l T^{kl} \tag{105}$$

Applying the curl gives

$$\partial_t \pi_T^i = -\epsilon_{ijk}\partial_j \partial_l \pi^{kl} \tag{106}$$

where we defined $\pi_T^i = \epsilon_{ijk}\partial_j T^{k0}$. Applying $(\partial_t + 1/\tau_\pi)$ and using Eq. (84) yields

$$0 = (\tau_\pi \partial_t^2 + \partial_t - D_T \nabla^2)\pi_T^i. \tag{107}$$

As long as $D_T/\tau_\pi < 1$, this is now causal.

For the sound modes, we start with the conservation law in the local rest frame

$$\partial_t^2 \varepsilon = \nabla^2 P + \partial_l \partial_m \pi^{lm} - \nabla^2 \Pi. \tag{108}$$

Applying $(\tau_\pi \partial_t + 1)(\tau_\Pi \partial_t + 1)$ to Eq. (108) and using Eqs. (101) and (102), one obtains the following dispersion relation for the bulk mode propagation (in this case $\delta\varepsilon$):

$$\begin{aligned} 0 = {} & \tau_\pi \tau_\Pi \omega^4 - \tau_\pi \tau_\Pi v_s^2 \omega^2 \mathbf{k}^2 - \tau_\Pi \frac{4D_T}{3}\mathbf{k}^2\omega^2 - \tau_\pi \gamma \mathbf{k}^2 \omega^2 \\ & - \omega^2 + v_s^2 \mathbf{k}^2 - i\left(\frac{4D_T}{3} + \gamma + v_s^2(\tau_\pi + \tau_\Pi)\right)\mathbf{k}^2\omega + i\omega^3(\tau_\pi + \tau_\Pi). \end{aligned} \tag{109}$$

Comparing with the small ω and small $|\mathbf{k}|$ expansion of the denominator in Eq. (80), we can identify $Z_R(0,0) = v_s^2$,

$$Z_I(0,0) = \frac{4D_T}{3} + \gamma + v_s^2(\tau_\pi + \tau_\Pi) \tag{110}$$

and

$$R_R(0,0) = (\tau_\pi + \tau_\Pi)/v_s^2. \tag{111}$$

The Kubo formula for the damping constant now makes more sense

$$\begin{aligned} \lim_{\omega\to 0}\lim_{\mathbf{k}\to 0} \mathrm{Im}\,\frac{\bar{G}_L(\omega,\mathbf{k})}{\omega} &= (\varepsilon + P)(Z_I(0,0) - Z_R(0,0)^2\, R_R(0,0)) \\ &= (\varepsilon + P)\left(\frac{4D_T}{3} + \gamma\right) \\ &= \frac{4\eta}{3} + \zeta \end{aligned} \tag{112}$$

and for the bulk viscosity only,

$$\zeta = \lim_{\omega\to 0}\lim_{\mathbf{k}\to 0} \frac{1}{\omega}\left(\mathrm{Im}\,\bar{G}_L(\omega,\mathbf{k}) - \frac{4}{3}\mathrm{Im}\,\bar{G}_R^{xy,xy}(\omega,k_y)\right). \tag{113}$$

The Kubo formula for the bulk viscosity ζ is also available in terms of the pressure–pressure correlation function[20,21]

$$\zeta = \lim_{\omega\to 0}\lim_{\mathbf{k}\to 0} \frac{1}{\omega}\mathrm{Im}\,G_R^{PP}(\omega,\mathbf{k}). \tag{114}$$

Using the fact that the correlation functions of T^{00} vanishes in the $\mathbf{k} \to 0$ limit, one can use in place of P the trace $T^\mu_\mu/3$ or the combination $P - v_s^2\varepsilon$ to make it more explicit that the bulk viscosity is non-zero only if the conformal symmetry is broken. The Kubo formulas for the relaxation times τ_π and τ_Π are not simple to determine in this analysis. Simple Kubo formulas for τ_π has been worked out in Refs. 25 and 26 as

$$\eta\tau_\pi = -\lim_{\omega\to 0}\lim_{\mathbf{k}\to 0}\frac{1}{2}\mathrm{Re}\,\partial_\omega^2 G_R^{xy,xy}(\omega,\mathbf{k}) \tag{115}$$

although a simple Kubo formula for τ_Π is still to be found.

In the dispersion relation Eq. (109), the fourth-order terms of $O(\omega^4)$ and $O(\omega^2\mathbf{k}^2)$ are present but $O(\mathbf{k}^4)$ terms are not. This may seem unsatisfactory since there is no reason why this term should be small compared to the other two fourth-order terms when $\omega \sim v_s|\mathbf{k}|$. However, one should recall that hydrodynamics is valid only in the long wavelength and small frequency limits. From this point of view, the fourth-order terms are not so important. They become, however, significant when the equations are solved numerically that can include short wavelength excitations. Fortunately, this Israel–Stewart form of second-order hydrodynamics[27] (comprising of Eqs. (96), (101) and (102)) is shown to be stable in Refs. 28 and 29.

If one wants to include $O(\mathbf{k}^4)$ terms, then one can modify the relaxation equations (101) and (102) to include second derivatives of T^{ij}. However, doing so not only generates $O(\mathbf{k}^4)$ terms, but it also generates (incomplete) terms involving 5 and 6 factors of ω and $\mathbf{k}$. Since higher order terms begin to matter at large ω and $|\mathbf{k}|$, having higher and higher order of frequency and momentum (or derivatives in the configuration space) does not guarantee that the numerical solution in this limit becomes more and more faithful to the real spectrum. One just needs to be careful not to interpret high frequency and momentum modes as physical.

As for the calculation of the viscosities, full leading order perturbative QCD results for both the shear viscosity and the bulk viscosity have been obtained in Refs. 30–32 using the Kubo formulas illustrated above. QCD is an asymptotically free theory.[33–35] In principle, it admits a perturbative expansion only when the energy scale exceeds at least a few GeV. Since the typical QGP energy scale is less than 1 GeV, the strong coupling is not small. Phenomenologically, we must have $\alpha_S \approx 0.3$.[36,37] This value may look weak, but the gauge coupling itself $g = \sqrt{4\pi\alpha_S} \approx 2$ is not so small. In the perturbative many-body QCD, g (or $g/2\pi$) is the expansion parameter not α_S.[38–41] Therefore although the analysis performed in Refs. 30–32 are nothing short of tour de force, having $g \approx 2$ makes numerical values obtained in perturbation theory not too reliable. At this point, reliable first principle calculations at large g can only be performed on numerical lattice in Euclidean space. Lattice QCD can straightforwardly compute static properties such as the equation of state. However, calculations of dynamic properties such as the viscosities become more complicated as they involve estimating real continuous functions from a finite set of discrete Euclidean data. Nonetheless, a great deal has been accomplished in computing the properties of QGP through lattice QCD

calculations[42–46] as well as through effective models such as the hadron resonance gas model (HR)[47,48] and the AdS/CFT correspondence.[6,49–51]

The purpose of this section has been to show that the hydrodynamics is very general. No matter what the system is, there usually is a regime where hydrodynamics is in some way applicable as long as there exist "macroscopically small but microscopically large" length and time scales. For more detailed analysis of the length and time scales and also for demonstrating more general structure of hydrodynamic equations, we now turn to the kinetic theory.

4. Hydrodynamics from Kinetic Theory

4.1. *Length scales and validity of hydrodynamic approximations*

Kinetic theory describes a medium microscopically, by following the evolution of the phase-space distribution function $f(x,p)$, a Lorentz scalar that describes the probability of finding a particle with four-momentum p^μ at space-time position x^ν. Classical kinetic theory assumes that the particle momenta are on-shell, $p^2 = m^2$, which requires the system to be sufficiently dilute and the mean free paths sufficiently long to ignore collisional broadening effects on the spectral function $\rho(p) = 2\pi\delta(p^2 - m^2)$ that defines the particles' propagator. The defining equation of classical kinetic theory is the Boltzmann equation,

$$p^\mu \partial_\mu f(x,p) = C(x,p), \tag{116}$$

where $C(x,p)$ is the collision term in which the strength of the interaction enters through their scattering cross-sections. Especially for massless degrees of freedom, its detailed form can be quite complicated.[52] A popular simplification of the collision term is the relaxation time approximation (RTA)[d]

$$C(x,p) = \frac{p^\mu u_\mu(x)}{\tau_{\rm rel}(x,p)}\,[f_{\rm eq}(x,p) - f(x,p)], \tag{117}$$

where the relaxation time $\tau_{\rm rel}$ in general depends on position through the local density and can also depend on the local rest frame energy of the particles (indicated by the p-dependence). Classical kinetic theory is valid if this relaxation time $\tau_{\rm rel}$, and the associated mean free path $\lambda_{\rm mfp} = \langle (p/E)\tau_{\rm rel}\rangle$, are sufficiently large. In other words, interactions among the constituents must be weak.

Hydrodynamics is valid if the system is close enough to thermal equilibrium that its local momentum distribution (and therefore its macroscopic fields, such as particle and energy density and pressure, which can all be expressed as moments of the local momentum distribution) can be characterized by a small number of thermodynamic and transport parameters, such as temperature, chemical potential, shear and bulk viscosity, etc. This requires efficient interactions among the constituents

[d]The Boltzmann equation with this RTA-approximated collision term is known as the Anderson–Witting equation.

of the medium because otherwise any kind of macroscopic dynamics involving local expansion or compression or shear of the fluid will drive its local momentum distribution away from its near-equilibrium form. Hydrodynamics works best for systems made of strongly interacting constituents.

Does this mean that the validity of kinetic theory and hydrodynamics are mutually exclusive? Not necessarily. To gain clarity consider a relativistic system of (almost) massless degrees of freedom. It can be characterized by three length scales, two microscopic and one macroscopic one:

- the thermal wavelength $\lambda_{\rm th} \sim 1/T$;
- the mean free path $\lambda_{\rm mfp} \sim 1/(\langle\sigma v\rangle n)$ where $\langle\sigma v\rangle$ is the momentum-averaged transport cross-section times the relative speed (≈ 1 in units of c) of the colliding objects, and n is the density of scatterers;
- the length scale $L_{\rm hydro}$ over which macroscopic fluid dynamical variables vary; it can be defined in many ways that give quantitatively different but similar order of magnitude results: $L^{-1}_{\rm hydro} \sim \partial_\mu u^\mu \sim |\partial_\mu e|/e$, etc.

The ratio between the two microscopic scales characterizes the magnitude of the transport coefficients η (shear viscosity), ζ (bulk viscosity), and κ (heat conductivity):

$$\frac{\lambda_{\rm mfp}}{\lambda_{\rm th}} \sim \frac{1}{\langle\sigma\rangle n}\,\frac{1}{\lambda_{\rm th}} \sim \frac{1}{\langle\sigma\rangle\lambda_{\rm th}}\,\frac{1}{s} \sim \frac{\eta}{s},\ \frac{\zeta}{s},\ \frac{T\kappa}{s}, \tag{118}$$

where we used $\eta,\ \zeta,\ T\kappa \sim 1/(\langle\sigma\rangle\lambda_{\rm th}) \sim \lambda_{\rm mfp}T^4$ and the entropy density $s \simeq 4n \sim T^3$ for a near-thermalized system of particle number density n for massless degrees of freedom.

In terms of the two microscopic length scales, we can define three regimes of microscopic dynamics:

(1) **Dilute gas regime**:

$$\frac{\lambda_{\rm mfp}}{\lambda_{\rm th}} \sim \frac{\eta}{s} \gg 1 \Leftrightarrow \langle\sigma\rangle \ll \lambda^2_{\rm th} \sim \frac{1}{T^2}. \tag{119}$$

This is the *weak-coupling regime* where the microscopic system dynamics can be described in terms of on-shell quasi-particles and many-body correlations are suppressed. In this regime the Boltzmann equation applies.

(2) **Dense gas regime**:

$$\frac{\lambda_{\rm mfp}}{\lambda_{\rm th}} \sim \frac{\eta}{s} \sim 1 \Leftrightarrow \langle\sigma\rangle \sim \lambda^2_{\rm th}. \tag{120}$$

In this case interactions happen on the scale $\lambda_{\rm th}$. We call this the *moderate coupling regime* where the microscopic system dynamics must be described by off-shell quasiparticles (whose spectral functions have a finite collisional width) and many-body correlation effects are non-negligible. Here the Boltzmann equation must be replaced by a quantum kinetic approach based on Wigner distributions,

and the BBGKY hierarchy of coupled equations for the N-body distribution functions can no longer be efficiently truncated.

(3) **Liquid regime**:

$$\frac{\lambda_{\rm mfp}}{\lambda_{\rm th}} \sim \frac{\eta}{s} \ll 1 \Leftrightarrow \langle\sigma\rangle \gg \lambda_{\rm th}^2. \tag{121}$$

This is the *strong-coupling regime* where the system has no well-defined quasi-particles and no valid kinetic theory description.

To judge the validity of a macroscopic hydrodynamic approach we compare the microscopic to the macroscopic length scales. To simplify the discussion, let us agree on using the inverse of the scalar expansion rate $\theta = \partial_\mu u^\mu$ to represent the macroscopic length scale $L_{\rm hydro}$.[e] The figure of merit controlling the validity of a fluid dynamic picture is the *Knudsen number*:

$$\mathrm{Kn} = \lambda_{\rm mfp} \cdot \theta \sim \frac{\eta}{s}\lambda_{\rm th} \cdot \theta \sim \frac{\eta}{sT} \cdot \theta \sim \theta\tau_{\rm rel}. \tag{122}$$

The Knudsen number is the small parameter that controls the convergence of the expansion in gradients of thermodynamic quantities that underlies the derivation of hydrodynamics as an effective theory for the long-distance dynamics of a general quantum field theory.[53] Again, we can use it to define three regimes:

(1) **Ideal fluid dynamics:**

$$\mathrm{Kn} \approx 0 \Leftrightarrow \frac{\eta}{s} \approx 0 \text{ or } \theta \approx 0 \text{ such that } \theta\tau_{\rm rel} \approx 0. \tag{123}$$

(2) **Viscous fluid dynamics:**

$$\mathrm{Kn} \lesssim 1 \Leftrightarrow \frac{\eta}{s} \text{ or } \theta \text{ small such that } \theta\tau_{\rm rel} \lesssim 1. \tag{124}$$

(3) **Hydrodynamics breaks down:**

$$\mathrm{Kn} \gg 1 \Leftrightarrow \frac{\eta}{s} \text{ or } \theta \text{ large such that } \theta\tau_{\rm rel} \gg 1. \tag{125}$$

In high-energy heavy-ion collisions, the initial energy deposition occurs in an approximately boost-invariant fashion along the beam direction, leading to an expansion rate θ that diverges like $1/\tau$ for small time τ after impact.[f] On the other hand we now know that the quantum mechanical uncertainty relation places a lower bound $\eta/s \gtrsim 1/(4\pi)$ on any system, even at infinitely strong coupling.[6,54,55] Therefore, hydrodynamics is inapplicable during the earliest stage of a heavy-ion collision. At the end of a heavy-ion collision, the mean free paths of hadrons become

[e]The shorter $L_{\rm hydro}$, the faster the system is driven away from local equilibrium. The scalar expansion rate directly drives the bulk viscous pressure Π. It is parametrically of the same order as the shear tensor $\sigma^{\mu\nu} = \Delta^{\mu\nu}_{\alpha\beta}\partial^\alpha u^\beta \equiv \nabla^{\langle\mu}u^{\nu\rangle}$ defined in Eq. (70) that drives the shear viscous pressure $\pi^{\mu\nu}$ and as the diffusion force $I^\mu = \nabla^\mu(\mu/T)$ associated with space-time gradients of conserved charge densities that drives the heat flow V^μ.

[f]Here, $\tau = \sqrt{t^2 - z^2}$ is the longitudinal proper time and the boost-invariance refers to independence of the space-time rapidity $\eta = \tanh^{-1}(z/t)$. For more details, see Sec. 5.1.

large compared to the Hubble radius $\sim 1/\theta$ of the expanding fireball, and hydrodynamics breaks down again. This process is called *kinetic decoupling*. Between the early pre-equilibrium and the final decoupling stage stretches an extended period of applicability of viscous fluid dynamics. The most important factor ensuring this is the strong collective coupling of the quark–gluon plasma (QGP) phase which is characterized by a small specific shear viscosity $\eta/s \sim (2-3)/(4\pi)$.[56–59]

Note that the validity of hydrodynamics does not rely directly on η/s being small, only on $(\eta/s)\cdot(\theta/T)$ being small. So, strictly speaking, strong coupling is not required for hydrodynamics to be valid. Only in extreme situations, such as heavy-ion collisions which are characterized by extreme expansion rates, does hydrodynamics require very strong coupling. In this case, hydrodynamics is applicable even though classical kinetic theory is not, because very strongly coupled quantum field theories do not allow a description in terms of on-shell quasi-particles. It is generally believed that the very earliest stage of a heavy-ion collision has no well-defined quasiparticles at all and is better described by a theory of classical or quantum fields than by a (quantum) kinetic approach. On the other hand, weakly coupled system, with very large values of η/s in which the applicability of (even classical) kinetic theory is ensured, can still be describable macroscopically through fluid dynamics if they are sufficiently homogeneous and expand slowly. In this case the smallness of θ can compensate for the largeness of η/s, resulting in a small Knudsen number. Systems with a large η/s but a small product $(\eta/s)\cdot(\theta/T)$ admit simultaneous microscopic classical kinetic and macroscopic hydrodynamic descriptions. In the following subsections we will study such systems to derive the macroscopic hydrodynamic equations from the microscopic kinetic theory. Hydrodynamics being an effective long-distance theory, the form of the resulting equations does not rely on the validity of the underlying kinetic theory (although the values for the transport coefficients do); they can therefore also be applied to a strongly-coupled liquid such as the QGP.

4.2. *Ideal fluid dynamics*

We define p-moments of the distribution function weighted with some momentum observable $O(p)$ by

$$\langle O(p)\rangle \equiv \int_p O(p) f(x,p) \equiv g \int \frac{d^3p}{(2\pi)^3 p^0} O(p) f(x,p) \tag{126}$$

(g is a degeneracy factor) and $p^0 = E_p = \sqrt{m^2+\mathbf{p}^2}$. The particle number current and energy momentum tensor are then written as

$$j^\mu = \langle p^\mu \rangle, \quad T^{\mu\nu} = \langle p^\mu p^\nu \rangle. \tag{127}$$

Usually there is more than one particle species in the system, and the conserved baryon charge current J^μ_B and energy–momentum tensor $T^{\mu\nu}$ are given in terms of

linear combinations of $\langle p^\mu \rangle_i$ and $\langle p^\mu p^\nu \rangle_i$ where the subscript i labels the particle species whose distribution function is $f_i(x,p)$:

$$J_B^\mu = \sum_i b_i j_i^\mu = \sum_i b_i \langle p^\mu \rangle_i, \quad T^{\mu\nu} = \sum_i T_i^{\mu\nu} = \sum_i \langle p^\mu p^\nu \rangle_i; \tag{128}$$

here b_i is the baryon charge carried by each particle of species i. For simplicity, we restrict the following discussion to a single particle species.

The particle number current and energy–momentum tensor take their ideal fluid dynamical form

$$j_{\rm id}^\mu = n u^\mu, \quad T_{\rm id}^{\mu\nu} = \varepsilon u^\mu u^\nu - P\Delta^{\mu\nu}, \tag{129}$$

where the spatial projector in the local rest frame (LRF) $\Delta^{\mu\nu}$ is given in Eq. (9), if we assume that the system is locally momentum isotropic:

$$f(x,p) = f_{\rm iso}(x,p) \equiv f_{\rm iso}\left(\frac{p^\mu u_\mu(x) - \mu(x)}{T(x)}\right). \tag{130}$$

The local equilibrium distribution

$$f_{\rm eq}(\zeta) = \frac{1}{e^\zeta + a}, \tag{131}$$

where $\zeta \equiv (p^\mu u_\mu(x) - \mu(x))/T(x)$ and $a = 1, -1, 0$ for Fermi–Dirac, Bose–Einstein, and classical Boltzmann statistics, respectively, is a special form of $f_{\rm iso}(x,p)$. It is defined as the distribution for which the collision term $C(x,p)$ in the Boltzmann equation (116) vanishes. Note that the ideal fluid decomposition (129) does not require chemical equilibrium, i.e., it holds for arbitrary values of the chemical potential $\mu(x)$, nor does it require complete thermal equilibrium, i.e., $f_{\rm iso}$ is not required to depend on its argument exponentially as is the case for the equilibrium distribution (131). If the dependence is non-exponential, the collision term in the Boltzmann equation is non-zero, but its p^μ-moment still vanishes, $\int_p p^\mu C = 0$, due to energy–momentum conservation.

The ideal hydrodynamic equations follow by inserting the ideal fluid decomposition (129) into the conservation laws Eq. (1):

$$\dot{n} = -n\theta, \quad \dot{\varepsilon} = -(\varepsilon + P)\theta, \quad \dot{u}^\nu = \frac{\nabla^\mu P}{\varepsilon + P} = \frac{c_s^2}{1 + c_s^2}\frac{\nabla^\mu \varepsilon}{\varepsilon}, \tag{132}$$

where the very last expression assumes an EOS of type $P = c_s^2 \varepsilon$. $\dot{F}$ denotes the LRF time derivative of a function F, $\dot{F} \equiv D_\tau F \equiv u^\mu \partial_\mu F$, and $\nabla^\mu = \Delta^{\mu\nu}\partial_\nu$ the spatial gradient in the LRF. Thus, $\partial_\mu = u^\mu D_\tau + \nabla^\mu$.[g]

Equations (132) can be solved numerically for the local particle density $n(x)$, energy density $\varepsilon(x)$, and flow velocity $u^\mu(x)$, with the temperature $T(x)$, chemical potential $\mu(x)$ and pressure $P(x)$ following from the equation of state (EOS) of the fluid. Local deviations from chemical equilibrium result in a non-equilibrium

[g]Note that in curvilinear coordinates or curved space-times, the partial derivative ∂_μ must be replaced by the covariant derivative d_μ.

value of the local chemical potential $\mu(x)$ and a non-zero right-hand side in the current conservation equation for j^μ. Deviations from thermal equilibrium (while preserving local isotropy) must be accounted for by a non-equilibrium pressure in the EOS $P(\varepsilon, n)$. In both cases, the conservation laws, Eqs. (1), lead to a non-vanishing entropy production rate $\partial_\mu S^\mu \sim 1/\tau_{\rm rel} \neq 0$.

4.3. *Viscous fluid dynamics*

4.3.1. *Navier–Stokes (NS), Israel–Stewart (IS) and Denicol–Niemi–Molnar–Rischke (DNMR) theory* (vHydro)

Israel–Stewart (IS) and Denicol–Niemi–Molnar–Rischke (DNMR) second-order viscous fluid dynamics[27] are obtained by using in (127) for $f(x,p)$ the ansatz

$$f(x,p) = f_{\rm iso}\left(\frac{p^\mu u_\mu(x) - \mu(x)}{T(x)}\right) + \delta f(x,p). \tag{133}$$

The correction δf describes the deviation of the solution $f(x,p)$ of the Boltzmann equation from local momentum isotropy. It is supposed to be "small", in a sense that will become clearer below, and will thus be treated perturbatively.

Most authors set $f_{\rm iso} = f_{\rm eq}$, i.e., they expand around a local equilibrium state. To obtain the correct form of the hydrodynamic equations this is not necessary; only the form of the equation of state $P(\varepsilon, n)$ and the values of the transport coefficients depend on this choice. We, too, will make this choice for simplicity, but emphasize that under certain conditions the perturbative treatment of δf may be better justified if the leading-order distribution $f_{\rm iso}$ is not assumed to be thermal.

For later convenience we decompose p^μ into its temporal and spatial components in the LRF:

$$p^\mu = (u^\mu u^\nu + \Delta^{\mu\nu})p^\mu = \bar{E}_p u^\mu + p^{\langle\mu\rangle} \tag{134}$$

where $\bar{E}_p \equiv u_\mu p^\mu$ and $p^{\langle\mu\rangle} \equiv \Delta^{\mu\nu} p_\nu$ are the energy and spatial momentum components in the LRF. Then

$$n = \langle \bar{E}_p \rangle, \quad \varepsilon = \langle \bar{E}_p^2 \rangle. \tag{135}$$

The decomposition (133) is made unique by Landau matching: First, define the LRF by solving the eigenvalue equation (7) with the constraint $u^\mu u_\mu = 1$ which selects among the four eigenvectors of $T^{\mu\nu}$ the timelike one. Equation (7) fixes the flow vector $u^\mu(x)$ and the LRF energy density. Next, we fix $T(x)$ and $\mu(x)$ by demanding that δf gives no contribution to the local energy and baryon density:

$$\langle \bar{E}_p \rangle_\delta = \langle \bar{E}_p^2 \rangle_\delta = 0. \tag{136}$$

Inserting (133) into (127) we find the general decomposition

$$j^\mu = j^\mu_{\rm id} + V^\mu, \quad T^{\mu\nu} = T^{\mu\nu}_{\rm id} - \Pi\Delta^{\mu\nu} + \pi^{\mu\nu}, \tag{137}$$

with a non-zero number flow in the LRF,

$$V^\mu = \langle p^{\langle\mu\rangle}\rangle_\delta, \tag{138}$$

a bulk viscous pressure

$$\Pi = -\frac{1}{3}\langle p^{\langle\alpha\rangle} p_{\langle\alpha\rangle}\rangle_\delta, \tag{139}$$

and a shear stress

$$\pi^{\mu\nu} = \langle p^{\langle\mu} p^{\nu\rangle}\rangle_\delta, \tag{140}$$

where $\langle\cdots\rangle_\delta$ indicates moments taken with the deviation δf from $f_{\rm iso}$. In the last equation we introduced the notation

$$A^{\langle\mu\nu\rangle} \equiv \Delta^{\mu\nu}_{\alpha\beta} A^{\alpha\beta}, \tag{141}$$

where $\Delta^{\mu\nu}_{\alpha\beta}$ is the spin-2 projector introduced in Eq. (71) denoting the traceless and transverse (to u^μ) part of a tensor $A^{\mu\nu}$. The shear stress tensor $\pi^{\mu\nu} = T^{\langle\mu\nu\rangle}$ thus has 5 independent components while V^μ, which is also orthogonal to u^μ by construction, has 3 independent components.

Using the viscous hydrodynamic decomposition (137) in the conservation laws $\partial_\mu T^{\mu\nu} = 0$ and $\partial_\mu j^\mu = 0$, we obtain the vHydro viscous hydrodynamic evolution equations

$$\begin{aligned} \dot{n} &= -n\theta - \nabla_\mu V^\mu, \\ \dot{\varepsilon} &= -(\varepsilon + P + \Pi)\theta + \pi_{\mu\nu}\sigma^{\mu\nu}, \\ (\varepsilon + P + \Pi)\dot{u}^\mu &= \nabla^\mu(P + \Pi) - \Delta^{\mu\nu}\nabla^\sigma \pi_{\nu\sigma} + \pi^{\mu\nu}\dot{u}_\nu, \end{aligned} \tag{142}$$

where $\sigma^{\mu\nu} = \nabla^{\langle\mu} u^{\nu\rangle}$ is the velocity shear tensor introduced in Eq. (70). They differ from the ideal fluid dynamical equations (132) by additional source terms arising from the dissipative flows. Altogether, the deviation δf has introduced $(3 + 1 + 5) = 9$ additional dissipative flow degrees of freedom for which additional evolution equations are needed. These cannot be obtained from the macroscopic conservation laws but require input from the microscopic dynamics. In a system that is initially in local equilibrium, the deviation δf is caused by the dynamical response of the system to gradients in the thermodynamic and flow variables. The forces that drive this deviation can be classified by their Lorentz structure as a scalar, a vector and a tensor force:

$$\begin{aligned} \text{scalar force:} \quad & \theta = \partial_\mu u^\mu \text{ (scalar expansion rate)}; \\ \text{vector force:} \quad & I^\mu = \nabla^\mu\left(\frac{\mu}{T}\right) \text{ (fugacity gradient)}; \\ \text{symmetric tensor force:} \quad & \sigma^{\mu\nu} = \nabla^{\langle\mu} u^{\nu\rangle} \text{ (velocity shear tensor)}; \\ \text{antisymmetric tensor force:} \quad & \omega^{\mu\nu} = \frac{1}{2}(\nabla^\mu u^\nu - \nabla^\nu u^\mu) \text{ (vorticity tensor)}. \end{aligned} \tag{143}$$

These forces generate dissipative flows, the scalar bulk viscous pressure Π, the heat flow vector V^μ, and the shear stress tensor $\pi^{\mu\nu}$.[h] The strength of the forces (143) driving the system away from local equilibrium is characterized by the Knudsen number. The system response can be characterized by inverse Reynolds numbers associated with the dissipative flows[60]:

$$\mathrm{R}_\Pi^{-1} = \frac{|\Pi|}{P}, \quad \mathrm{R}_V^{-1} = \frac{\sqrt{-I_\mu I^\mu}}{P}, \quad \mathrm{R}_\pi^{-1} = \frac{\sqrt{\pi_{\mu\nu}\pi^{\mu\nu}}}{P}. \tag{144}$$

Due to the time delay $\tau_{\rm rel}$ between the action of the force and the system response, built into the collision term of the Boltzmann equation, the inverse Reynolds numbers are not necessarily of the same order as the Knudsen number: For example, an initially small bulk viscous pressure can remain small, due to critical slowing down, as the system passes through a phase transition, even though the bulk viscosity becomes large during the transition.[61] Conversely, strong deviations from local equilibrium during a rapidly expanding pre-equilibrium stage in heavy-ion collisions can lead to large initial values for the dissipative flows, and a slow equilibration rate may cause them to stay large for a while even though the expansion rate decreases with longitudinal proper time as $1/\tau$. Deviations from equilibrium, and the accuracy of their description by viscous fluid dynamics, are therefore controlled by a combination of Knudsen and inverse Reynolds numbers.[60]

The 9 equations of motion describing the relaxation of the 9 dissipative flow components are controlled by microscopic physics, encoded in the collision term on the right-hand side of the Boltzmann equation, and can be derived from approximate solutions of that equation. This was first done almost 50 years ago by Israel and Stewart in Ref. 27, but when the problem was recently revisited it was found[25,60,62,63] that the relaxation equations take a much more general form than originally derived. Specifically, Denicol *et al.*[60] found the following general structure:

$$\begin{aligned}
\tau_\Pi \dot\Pi + \Pi &= -\zeta\theta + \mathcal{J} + \mathcal{K} + \mathcal{R}, \\
\tau_V \Delta^{\mu\nu}\dot V_\nu + V^\mu &= \kappa I^\mu + \mathcal{J}^\mu + \mathcal{K}^\mu + \mathcal{R}^\mu, \\
\tau_\pi \Delta^{\mu\nu}_{\alpha\beta}\dot\pi^{\alpha\beta} + \pi^{\mu\nu} &= 2\eta\sigma^{\mu\nu} + \mathcal{J}^{\mu\nu} + \mathcal{K}^{\mu\nu} + \mathcal{R}^{\mu\nu}.
\end{aligned} \tag{145}$$

Here all calligraphic terms are of second-order in combined powers of the Knudsen and inverse Reynolds numbers. $\mathcal{J}$ terms contain products of factors that are each of first-order in the Knudsen and inverse Reynolds numbers; $\mathcal{K}$ terms are second-order in Knudsen number, and $\mathcal{R}$ terms are second-order in inverse Reynolds numbers.

In relaxation time approximation, with an energy-independent relaxation time $\tau_{\rm rel}$, the relaxation times for the dissipative flows all agree with each other: $\tau_\Pi = \tau_V = \tau_\pi = \tau_{\rm rel}$.[63] The same does not hold for more general forms of the collision

[h]The energy–momentum tensor is symmetric, so dissipative flows have no antisymmetric tensor contribution, but the antisymmetric vorticity tensor couples to the other dissipative forces and flows at second-order in the Knudsen and inverse Reynolds numbers.

term. If we set in Eqs. (145) the relaxation times and all other second-order terms to zero, we obtain the equations of **relativistic NS theory**:

$$\Pi = -\zeta\theta, \quad V^\mu = \kappa I^\mu, \quad \pi^{\mu\nu} = 2\eta\sigma^{\mu\nu}. \tag{146}$$

The relaxation equations (145) have solutions that, for sufficiently small expansion rates (see below), approach asymptotically (at times $\tau \gg \tau_{\Pi,V,\pi}$) the NS values (146). However, plugging the NS solutions (146) directly back into the decompositions (137) and using them in the conservation laws (1) leads to viscous hydrodynamic equations of motion that are acausal and numerically unstable.[64,65] The physical reason for this is the instantaneous response of the dissipative flows to the dissipative forces encoded in Eqs. (146) which violates causality. A causal and numerically stable implementation of viscous fluid dynamics must account for the time delay between cause and effect of dissipative phenomena and therefore be by necessity of second-order in Knudsen and Reynolds numbers.

The first relativistic causal second-order theory of viscous fluid dynamics was IS theory.[27] It amounts to dropping the $\mathcal{K}$ and $\mathcal{R}$ terms in (145) and replacing (for massless particles) $\mathcal{J} \to -\frac{4}{3}\tau_\Pi\theta\Pi$, $\mathcal{J}^\mu \to -\tau_V\theta V^\mu$, and $\mathcal{J}^{\mu\nu} \to -\frac{4}{3}\tau_\pi\theta\pi^{\mu\nu}$. The importance of keeping specifically these second-order $\mathcal{J}$-terms for the preservation of conformal invariance in a system of massless degrees of freedom was stressed by Baier *et al.*[25]

For conformal systems the resulting IS relaxation equations can be written in the form[66]

$$\begin{aligned}
\dot{\Pi} &= -\frac{1}{\tau'_\Pi}(\Pi + \zeta'\theta), \\
\Delta^{\mu\nu}\dot{V}_\nu &= -\frac{1}{\tau'_V}(V^\mu - \kappa' I^\mu), \\
\Delta^{\mu\nu}_{\alpha\beta}\dot{\pi}^{\alpha\beta} &= -\frac{1}{\tau'_\pi}(\pi^{\mu\nu} - 2\eta'\sigma^{\mu\nu}),
\end{aligned} \tag{147}$$

with effective transport coefficients and relaxation times that are modified by the scalar expansion rate as follows:

$$\zeta' = \frac{\zeta}{1+\gamma_\Pi}, \quad \kappa' = \frac{\kappa}{1+\gamma_V}, \quad \eta' = \frac{\eta}{1+\gamma_\pi}, \quad \tau'_i = \frac{\tau_i}{1+\gamma_i} \ (i = \Pi,\, V,\, \pi), \tag{148}$$

where $\gamma_i = \frac{4}{3}\theta\tau_i$ for $i = \Pi, \pi$ and $\gamma_i = \theta\tau_i$ for $i = V$. These relaxation equations describe an asymptotic approach of the dissipative flows to effective NS values that, for a positive scalar expansion rate θ, are reduced relative to their first-order values (146) by a factor $1+\gamma_i$, while the effective rate of approach to this effective NS limit is sped up by the same factor. γ_i involves the product of the scalar expansion rate and the respective relaxation time. So, compared to a more slowly expanding system, a rapidly expanding system with the same microscopic scattering cross-sections is characterized by lower effective viscosities and shorter effective relaxation times.[66,67]

When all the second-order terms are kept, the DNMR equations become quite complicated. The $\mathcal{J}$, $\mathcal{K}$ and $\mathcal{R}$ terms listed by DNMR[60] add up to 16 terms for Π, 18 terms for V^μ, and 19 terms for $\pi^{\mu\nu}$, each with its own transport coefficient. While many of these transport coefficients have been computed for massless theories at both weak and strong coupling (a subject too rich to be fully reviewed here, see papers by Denicol *et al.*,[60,63,68] Moore *et al.*[69,70] and Noronha *et al.*[71] for lists of references to relevant work), quite a few are still unknown. Furthermore, the QGP is neither weakly nor strongly enough coupled, nor is it sufficiently conformally symmetric for any of these calculations to be quantitatively reliable for heavy-ion collisions. For these reasons, many practical applications of viscous fluid dynamics employ phenomenological values for the transport coefficients, and work studying which terms need to be kept and which might be of lesser importance is still ongoing.[68]

One important non-linear coupling mechanism that enters at second-order are bulk-shear couplings where shear stress drives a bulk viscous pressure and vice versa.[60,63,68,72] Heavy-ion collisions are characterized by initially very large differences between the longitudinal and transverse expansion rates that cause large shear stress. The latter, in turn, creates a bulk viscous pressure via bulk-shear coupling that can dominate over the one generated *à la* NS by the scalar expansion rate[72] and may actually be able to flip its sign. This should be taken into account in phonemenological applications of viscous hydrodynamics to heavy-ion collisions.

4.3.2. *Anisotropic hydrodynamics* (aHydro)

The dissipative flows are given by moments of the deviation $\delta f(x,p)$ of the distribution function from local equilibrium, and their relaxation equations are derived from the Boltzmann equation using approximations that, in one way or another, assume that δf is small. However, systems featuring strongly anisotropic expansion, such as the early evolution stage of the fireballs created in ultra-relativistic heavy-ion collisions, generate strong local momentum anisotropies: the width of the LRF momentum distribution along a certain direction is inversely proportional to the local expansion rate in that direction, and this momentum-space distortion growth with the magnitude of the shear viscosity. In viscous hydrodynamics, where we expand f around a locally isotropic LO distribution (see Eq. (133)), this local momentum anisotropy must be absorbed entirely by δf, making δf large and rendering the approximations used for calculating the evolution of the dissipative flow generated by δf unreliable. Indeed, even for moderate specific shear viscosities $\eta/s \sim 5-10$ the (negative) longitudinal component of the viscous shear pressure can become so large in IS theory that it overwhelms the thermal pressure, resulting in a negative total pressure along the beam direction — which, according to the kinetic definition $P_L = \frac{1}{3}\langle p_z^2 \rangle$, should never happen.

Anisotropic hydrodynamics[73,74] is based on the idea to account already in the LO distribution for the local momentum anisotropy resulting from anisotropic expansion, by parametrizing[75]

$$f(x,p) = f_{\rm RS}(x,p) \equiv f_{\rm iso}\left(\frac{\sqrt{p_\mu \Xi^{\mu\nu}(x) p_\nu} - \tilde{\mu}(x)}{\Lambda(x)}\right), \tag{149}$$

where $\Xi^{\mu\nu}(x) = u^\mu(x)u^\nu(x) + \xi(x) z^\mu(x) z^\nu(x)$, $z^\mu(x)$ being a unit vector in longitudinal z direction in the LRF. The subscript RS refers to Romatschke and Strickland who are the authors of Ref. 75. This distribution is characterized by 3 flow parameters $u^\mu(x)$ and three "thermodynamic" parameters: the "transverse temperature" $\Lambda(x)$, the effective chemical potential $\tilde{\mu}(x)$, and the momentum-anisotropy parameter $\xi(x)$. Inserting (149) into (127) yields the aHydro decomposition

$$j^\mu_{\rm RS} = n_{\rm RS} u^\mu, \quad T^{\mu\nu}_{\rm RS} = \varepsilon_{\rm RS} u^\mu u^\nu - P_T \Delta^{\mu\nu} + (P_L - P_T) z^\mu z^\nu, \tag{150}$$

$$n_{\rm RS} = \langle E \rangle_{\rm RS} = \mathcal{R}_0(\xi)\, n_{\rm iso}(\Lambda, \tilde{\mu}), \quad \varepsilon_{\rm RS} = \langle E^2 \rangle_{\rm RS} = \mathcal{R}(\xi)\, \varepsilon_{\rm iso}(\Lambda, \tilde{\mu}),$$

$$P_{T,L} = \langle p^2_{T,L} \rangle_{\rm RS} = \mathcal{R}_{T,L}(\xi) P_{\rm iso}(\Lambda, \tilde{\mu}). \tag{151}$$

For massless systems, the local momentum anisotropy effects factor out via the $\mathcal{R}(\xi)$-functions[73]:

$$\begin{aligned} \mathcal{R}_0(\xi) &= \frac{1}{\sqrt{1+\xi}}, & \mathcal{R}(\xi) &= \frac{1}{2}\left(\frac{1}{1+\xi} + \frac{\arctan\sqrt{\xi}}{\sqrt{\xi}}\right), \\ \mathcal{R}_\perp(\xi) &= \frac{3}{2\xi}\left(\frac{1+(\xi^2-1)\mathcal{R}(\xi)}{\xi+1}\right), & \mathcal{R}_L(\xi) &= \frac{3}{\xi}\left(\frac{(\xi+1)\mathcal{R}(\xi)-1}{\xi+1}\right). \end{aligned} \tag{152}$$

The isotropic pressure is obtained from a locally isotropic equation of state $P_{\rm iso}(\Lambda, \tilde{\mu}) = P_{\rm iso}(\varepsilon_{\rm iso}(\Lambda, \tilde{\mu}), n_{\rm iso}(\Lambda, \tilde{\mu}))$. For massless noninteracting partons, $P_{\rm iso}(\Lambda, \tilde{\mu}) = \frac{1}{3}\varepsilon_{\rm iso}(\Lambda, \tilde{\mu})$ independent of chemical composition. To compare with ideal and IS viscous hydrodynamics, we need to assign the locally anisotropic system an appropriate temperature $T(x) = T(\xi(x), \Lambda(x), \tilde{\mu}(x))$ and chemical potential $\mu(x) = \mu(\xi(x), \Lambda(x), \tilde{\mu}(x))$, thinking of $f_{\rm RS}(\xi, \Lambda)$ as an expansion around the locally isotropic distribution $f_{\rm iso}(T)$. For this we impose the generalized Landau matching conditions $\varepsilon_{\rm RS}(\xi, \Lambda, \tilde{\mu}) = \varepsilon_{\rm iso}(T, \mu)$ and For example, using an exponential (Boltzmann) function for $f_{\rm iso}$ with $\mu = \tilde{\mu} = 0$, one finds $T = \Lambda \mathcal{R}^{1/4}(\xi)$. With this matching we can write

$$T^{\mu\nu}_{\rm RS} = T^{\mu\nu}_{\rm id} - (\Delta P + \Pi_{\rm RS})\Delta^{\mu\nu} + \pi^{\mu\nu}_{\rm RS}, \tag{153}$$

$$\Delta P + \Pi_{\rm RS} = -\frac{1}{3}\int_p p_\alpha \Delta^{\alpha\beta} p_\beta (f_{\rm RS} - f_{\rm iso}) \quad (= 0 \text{ for } m = 0), \tag{154}$$

$$\pi^{\mu\nu}_{\rm RS} = \int_p p^{\langle\mu} p^{\nu\rangle} (f_{\rm RS} - f_{\rm iso}) = (P_T - P_L)\, \frac{x^\mu x^\nu + y^\mu y^\nu - 2 z^\mu z^\nu}{3}. \tag{155}$$

We see that $\pi^{\mu\nu}_{\rm RS}$ has only one independent component, $P_T - P_L$, so aHydro leaves 4 of the 5 components of $\pi^{\mu\nu}$ unaccounted for. For massless particles

we have $(P_T - P_L)/P_{\rm iso}(\varepsilon) = \mathcal{R}_T(\xi) - \mathcal{R}_L(\xi)$, so the equation of motion for $\pi^{\mu\nu}_{\rm RS}$ can be replaced by one for ξ. For (2+1)-dimensional expansion with longitudinal boost-invariance these equations can be found and were solved numerically by Martinez *et al.*[76] For $m \neq 0$ we need an additional "anisotropic EOS" for $(\Delta P/P_{\rm iso}) \equiv (2P_T + P_L)/(3P_{\rm iso}) - 1$, in order to separate ΔP from the viscous bulk pressure Π.

4.3.3. *Viscous anisotropic hydrodynamics* (VAHYDRO)

As explained above, AHYDRO[73,74] accounts only for one (albeit largest) of the five independent components of the shear stress tensor $\pi^{\mu\nu}$. It can therefore not be used to compute the viscous suppression of elliptic flow which is sensitive to e.g., $\pi^{xx} - \pi^{yy}$. On the other hand, since the four remaining components of the shear stress tensor never become as large as the longitudinal/transverse pressure difference (with smooth initial density profiles they start out as zero, and with fluctuating initial conditions they are initially small), they can be treated "perturbatively" *à la* Israel and Stewart, without running into problems even at early times. Combining the non-perturbative dynamics of $P_L - P_T$ via AHYDRO with a perturbative treatment of the remaining viscous stress terms $\tilde\pi^{\mu\nu}$ *à la* IS defines the VAHYDRO scheme.[77] VAHYDRO is expected to perform better than both IS theory and AHYDRO during all evolution stages.

The VAHYDRO equations are obtained by generalizing the ansatz (149) to include arbitrary (but small) corrections to the spheroidally deformed $f_{\rm RS}(x,p)$:

$$\begin{aligned} f(x,p) &= f_{\rm RS}(x,p) + \delta\tilde f(x,p) \\ &= f_{\rm iso}\left(\frac{\sqrt{p_\mu \Xi^{\mu\nu}(x) p_\nu} - \tilde\mu(x)}{\Lambda(x)}\right) + \delta\tilde f(x,p). \end{aligned} \tag{156}$$

The parameters Λ and $\tilde\mu$ in (156) are Landau-matched as before, i.e., by requiring $\langle E\rangle_{\tilde\delta} = \langle E^2\rangle_{\tilde\delta} = 0$. To fix the value of the deformation parameter ξ one demands that $\delta\tilde f$ does not contribute to the pressure anisotropy $P_T - P_L$; this requires $(x_\mu x_\nu + y_\mu y_\nu - 2z_\mu z_\nu)\langle p^{\langle\mu} p^{\nu\rangle}\rangle_{\tilde\delta} = 0$. Then, upon inserting (156) into (127), we obtain the VAHYDRO decomposition

$$j^\mu = j^\mu_{\rm RS} + \tilde V^\mu, \quad T^{\mu\nu} = T^{\mu\nu}_{\rm RS} - \tilde\Pi\Delta^{\mu\nu} + \tilde\pi^{\mu\nu}, \tag{157}$$

with

$$\tilde V^\mu = \langle p^{\langle\mu\rangle}\rangle_{\tilde\delta}, \quad \tilde\Pi = -\tfrac{1}{3}\langle p^{\langle\alpha\rangle} p_{\langle\alpha\rangle}\rangle_{\tilde\delta}, \quad \tilde\pi^{\mu\nu} = \langle p^{\langle\mu} p^{\nu\rangle}\rangle_{\tilde\delta}, \tag{158}$$

subject to the constraints

$$u_\mu\tilde\pi^{\mu\nu} = \tilde\pi^{\mu\nu}u_\nu = (x_\mu x_\nu + y_\mu y_\nu - 2z_\mu z_\nu)\tilde\pi^{\mu\nu} = \tilde\pi^\mu_\mu = 0. \tag{159}$$

Clearly, the additional shear stress $\tilde\pi^{\mu\nu}$ arising from $\delta\tilde f$ has only 4 degrees of freedom.

The strategy in vaHydro is now to solve hydrodynamic equations for aHydro[76] (which treat $P_T - P_L$ non-perturbatively) with added source terms describing the residual viscous flows arising from $\delta\tilde{f}$, together with IS-like "perturbative" equations of motion for $\tilde{\Pi}$, $\tilde{V}^\mu$, and $\tilde{\pi}^{\mu\nu}$. The hydrodynamic equations are obtained by using the decomposition (157) in the conservation laws (1). The evolution equations for the dissipative flows $\tilde{\Pi}$, $\tilde{V}^\mu$, and $\tilde{\pi}^{\mu\nu}$ are derived by generalizing the DNMR[60] procedure to an expansion of the distribution function around the spheroidally deformed $f_{\rm RS}$ in (149), using the 14-moment approximation. These equations are lengthy; for massless systems undergoing $(2+1)$-dimensional expansion with longitudinal boost invariance they were derived by Bazow *et al.*[77] Generalizations to massive systems and full (3+1)-dimensional expansion are in progress. We give their simplified form for $(0+1)$-dimensional expansion in the next subsection. Especially at early times $\delta\tilde{f}$ is much smaller than δf, since the largest part of δf is already accounted for by the momentum deformation in (149). The inverse Reynolds number $\tilde{\rm R}_\pi^{-1} = \sqrt{\tilde{\pi}^{\mu\nu}\tilde{\pi}_{\mu\nu}}/\mathcal{P}_{\rm iso}$ associated with the residual shear stress $\tilde{\pi}^{\mu\nu}$ is therefore strongly reduced compared to the one associated with $\pi^{\mu\nu}$, significantly improving the range of applicability of vaHydro relative to standard second-order viscous hydrodynamics.

4.4. *Testing different hydrodynamic approximations*

For $(0+1)$-dimensional longitudinally boost-invariant expansion of a transversally homogeneous system, the Boltzmann equation can be solved exactly in the relaxation time approximation (RTA), both for massless[78–80] and massive particles.[81,82] More recently, an exact solution of this equation was also found for massless systems undergoing (1+1)-dimensional expansion,[83,84] with a boost invariant longitudinal and azimuthally symmetric transverse velocity profile discovered by Gubser ("Gubser flow")[85,86] as the result of imposing a particular conformal symmetry ("Gubser symmetry") on the flow. These exact solutions of the kinetic theory can be used to test various hydrodynamic approximation schemes, by imposing the symmetry of the exact solution also on the hydrodynamic solution, solving both with identical initial conditions, and comparing the predictions of both approaches for the evolution of macroscopic observables.[77,79,80,83,84,87]

We will here use the (0+1)-dimensional case to test the vaHydro approach.[77] This illustrates the procedure and the kind of conclusions one can draw from such a comparison. Setting homogeneous initial conditions in r and space-time rapidity η_s and zero transverse flow, $\tilde{\pi}^{\mu\nu}$ reduces to a single non-vanishing component $\tilde{\pi}$: $\tilde{\pi}^{\mu\nu} = {\rm diag}(0, -\tilde{\pi}/2, -\tilde{\pi}/2, \tilde{\pi})$ at $z = 0$. The factorization $n_{\rm RS}(\xi,\Lambda) = \mathcal{R}_0(\xi) n_{\rm iso}(\Lambda)$ etc. are used to obtain equations of motion for $\dot{\xi}$, $\dot{\Lambda}$, $\dot{\tilde{\pi}}$:[77]

$$\frac{\dot{\xi}}{1+\xi} - 6\frac{\dot{\Lambda}}{\Lambda} = \frac{2}{\tau} + \frac{2}{\tau_{\rm rel}}(1 - \sqrt{1+\xi}\,\mathcal{R}^{3/4}(\xi)),$$

$$\mathcal{R}'(\xi)\dot{\xi} + 4\mathcal{R}(\xi)\frac{\dot{\Lambda}}{\Lambda} = -\left(\mathcal{R}(\xi) + \frac{1}{3}\mathcal{R}_L(\xi)\right)\frac{1}{\tau} + \frac{\tilde{\pi}}{\varepsilon_{\rm iso}(\Lambda)\tau},$$
$$\dot{\tilde{\pi}} = -\frac{1}{\tau_{\rm rel}}[(\mathcal{R}(\xi) - \mathcal{R}_{\rm L}(\xi))P_{\rm iso}(\Lambda) + \tilde{\pi}] - \lambda(\xi)\frac{\tilde{\pi}}{\tau}$$
$$+ 12\left[\frac{\dot{\Lambda}}{3\Lambda}(\mathcal{R}_{\rm L}(\xi) - \mathcal{R}(\xi)) + \left(\frac{1+\xi}{\tau} - \frac{\dot{\xi}}{2}\right)\right.$$
$$\left.\times\left(\mathcal{R}^{zzzz}_{-1}(\xi) - \frac{1}{3}\mathcal{R}^{zz}_{1}(\xi)\right)\right]P_{\rm iso}(\Lambda). \tag{160}$$

$\tau_{\rm rel}$ and the ratio of shear viscosity η to entropy density s, η/s, are related by $\tau_{\rm rel} = 5\eta/(sT) = 5\eta/(\mathcal{R}^{1/4}(\xi)s\Lambda)$. The numerical solution of these equations[77] can be compared with the exact solution of the Boltzmann equation,[79] and also with the other hydrodynamic approximation schemes discussed above, plus a third-order viscous hydrodynamic approximation.[88] As an example, we show in Fig. 1 the entropy production (measured by the increase in particle number $\tau n(\tau)$) between start and end of the dynamical evolution from an initial temperature of 600 MeV to a final one of 150 MeV. For this extreme (0+1)-dimensional scenario, where the difference between longitudinal and transverse expansion rates is maximal, vaHydro is seen to reproduce the exact solution almost perfectly, dramatically outperforming all other hydrodynamic approximations. In particular, it should be noted that only the aHydro and vaHydro approximations are able to correctly reproduce entropy production (or rather the lack thereof) in both the extreme strong coupling (ideal

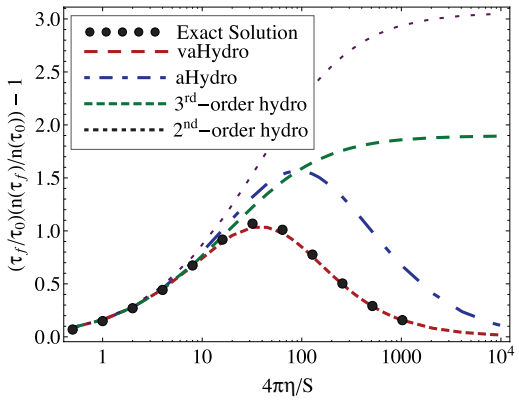

Fig. 1. (Color online) The particle production measure $(\tau_f n(\tau_f))/(\tau_0 n(\tau_0)) - 1$ as a function of $4\pi\eta/s$. The black points, red dashed line, blue dashed–dotted line, green dashed line, and purple dotted line correspond to the exact solution of the Boltzmann equation, vaHydro, aHydro, third-order viscous hydrodynamics,[88] and DNMR second-order viscous hydrodynamics,[60] respectively. The initial conditions are $T_0 = 600$ MeV, $\xi_0 = 0$, and $\tilde{\pi}_0 = 0$ at $\tau_0 = 0.25$ fm/c. The freeze-out temperature was taken to be $T_f = 150$ MeV.

fluid dynamics, $\tau_{\rm real} = \eta/s = 0$) and the extreme weak coupling (free-streaming particles, no collisions, $\tau_{\rm real}$, $\eta/s = \to \infty$) limits of the microscopic dynamics. vHydro schemes based on an expansion around a locally isotropic equilibrium distribution cannot reproduce the constraint that entropy production should vanish as collisions cease; these schemes break down for large η/s values.

Similar comparisons have been done for the massive (0+1)-dimensional case[81,82,89] and for the (1+1)-dimensional Gubser flow. In all cases one finds the following hierarchy of hydrodynamic approximations, when listed in order of improving accuracy in their descriptions of the moments of the exactly known microscopic dynamics: first-order viscous hydrodynamics (NS theory), second-order IS theory, second-order DNMR theory, third-order viscous hydrodynamics *à la* Jaiswal, aHydro, and vaHydro. In view of the increasing sophistication of these approximation schemes, as discussed in the preceding subsections, this ordering is not surprising, and some variant of vaHydro is likely to become the standard hydrodynamic modelling framework in the future. At the moment, however, only vHydro and aHydro have been implemented numerically for (2+1)-dimensional and (3+1)-dimensional expansion which do not rely on simplifying assumptions such as longitudinal boost-invariance and azimuthal symmetry. The fireballs created in heavy-ion collisions are not azimuthally symmetric, and experiments tell us that they feature characteristic anisotropic flow patterns that could never arise from an azimuthally symmetric initial condition. Longitudinal boost-invariance is not a good approximation either for particles emitted at large forward and backward rapidities, and it becomes worse when going to lower energies. Therefore, much effort is presently being expended into developing (2+1)-dimensional and (3+1)-dimensional implementations of the aHydro and vaHydro schemes.

5. Numerical Implementation of Hydrodynamics

5.1. *Need for τ and η*

The hydrodynamic simulations of the ultra-relativistic heavy ion collisions is best implemented in the hyperbolic coordinate system[90] (also known as the Milne coordinate system) where instead of t (the laboratory time) and z (the beam direction), one uses the longitudinal proper time

$$\tau = \sqrt{t^2 - z^2} \tag{161}$$

and the space-time rapidity

$$\eta = \tanh^{-1}(z/t). \tag{162}$$

Equivalently, $t = \tau \cosh \eta$ and $z = \tau \sinh \eta$.

One reason this is useful is that as shown in Fig. 2, the evolution of the ultra-relativistic heavy ion collisions can occur only in the forward light cone bounded by the light cone axes, equivalently $\tau = 0$. More physically, suppose two identical systems were created at $t = 0$ and $z = 0$ by the initial collision of the two nuclei.

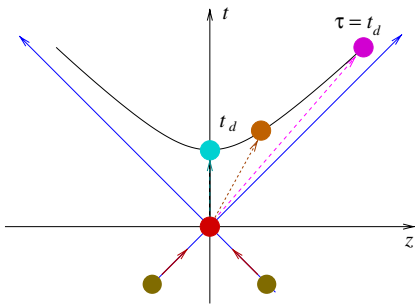

Fig. 2. A schematic diagram showing evolution of fireballs with differing v_z after the collision of two heavy ions at $t = 0$ and $z = 0$.

Further suppose that one of the two has the collective velocity v in the z direction, but the other one is at rest. In this case, due to the time dilation, the same stage of the evolution will be reached when the lab time is at t_d for the system at rest and at $t_d/\sqrt{1-v^2}$ for the moving system. In relativistic systems, these two Minkowski times can be very much different even though the two system are at the same stage in their respective evolution. However, in terms of the proper time both are at the same $\tau = t_d$ since τ is nothing but the local rest frame time. Hence, it is very natural that we should use the $\tau - \eta$ coordinate system when there is a strong longitudinal flow of matter. In the ultra-relativistic heavy ion collisions, this is the case due to the original beam momenta of the projectile and the target.

For numerical implementation of hydrodynamics, one first needs to formulate the conservation laws in this coordinate system. For this, we need to know the transformation law between $\tau - \eta$ and $t - z$. We can start with the derivatives

$$\begin{aligned}\partial_\tau &= \frac{\partial t}{\partial \tau}\partial_t + \frac{\partial z}{\partial \tau}\partial_z \\ &= \cosh\eta\partial_t + \sinh\eta\partial_z \end{aligned} \tag{163}$$

and

$$\begin{aligned}\partial_\eta &= \frac{\partial t}{\partial \eta}\partial_t + \frac{\partial z}{\partial \eta}\partial_z \\ &= \tau\sinh\eta\partial_t + \tau\cosh\eta\partial_z \end{aligned} \tag{164}$$

which can be summarized as Lorentz transformations

$$\tilde{\partial}_a = \Lambda^\mu_a \partial_\mu \quad \text{and} \quad \partial_\mu = \Lambda^a_\mu \tilde{\partial}_a \tag{165}$$

where $\tilde{\partial}_a = (\partial_\tau, \nabla_\perp, (1/\tau)\partial_\eta)$ and

$$\Lambda^a_\mu = \begin{pmatrix} \cosh\eta & 0 & 0 & -\sinh\eta \\ 0 & 1 & 0 & 0 \\ 0 & 0 & 1 & 0 \\ -\sinh\eta & 0 & 0 & \cosh\eta \end{pmatrix}. \tag{166}$$

The inverse transform Λ^μ_a is obtained by substituting η with $-\eta$. From now on, we will use the first letters of the roman alphabet $(a, b, \ldots)$ to represent the components in the Milne space as above.

To figure out the transformation of the conservation law, we apply Eq. (165) to

$$\begin{aligned}\partial_t j^0 + \partial_z j^3 &= \cosh\eta\partial_\tau j^0 - \frac{\sinh\eta}{\tau}\partial_\eta j^0 + \frac{\cosh\eta}{\tau}\partial_\eta j^3 - \sinh\eta\partial_\tau j^3 \\ &= \frac{1}{\tau}\partial_\tau(\tau\cosh\eta j^0 - \tau\sinh\eta j^3) \\ &\quad - \partial_\eta\left(\frac{1}{\tau}\sinh\eta j^0 - \frac{1}{\tau}\cosh\eta j^3\right). \end{aligned} \tag{167}$$

Defining

$$\begin{aligned} q^\tau &= \cosh\eta\, q^0 - \sinh\eta\, q^3, \\ \tilde{q}^\eta &= \cosh\eta\, q^3 - \sinh\eta\, q^0 \end{aligned} \tag{168}$$

and

$$\tilde{q}^a = (q^\tau, \mathbf{q}_\perp, \tilde{q}^\eta), \tag{169}$$

for any 4-vector q^μ, the conservation law becomes

$$0 = \partial_\tau(\tau j^\tau) + \nabla_\perp\cdot(\tau\mathbf{j}_\perp) + \partial_\eta\tilde{j}^\eta = \tilde{\partial}_a(\tau\tilde{j}^a) \tag{170}$$

where $\mathbf{j}_\perp$ only has the x, y components. One can also show

$$D_\tau = u^\mu\partial_\mu = \tilde{u}^a\tilde{\partial}_a. \tag{171}$$

Note that our definition of the η component is different from the curvilinear definition of the η component by a factor of τ. We do this to keep the dimension of the η component the same as the other components. If one uses the curvilinear definition

$$j^\eta = \frac{1}{\tau}\tilde{j}^\eta \tag{172}$$

then the conservation law becomes

$$0 = \partial_\tau(\tau j^\tau) + \nabla_\perp\cdot(\tau\mathbf{j}_\perp) + \partial_\eta(\tau j^\eta) = \partial_a(\tau j^a) \tag{173}$$

where $\partial_a = (\partial_\tau, \nabla_\perp, \partial_\eta)$.

For the energy–momentum conservation, one needs to apply the transformation law 3 times for the each index in $\partial_\mu T^{\mu\nu} = 0$. The algebra is a bit tedious but straightforward.[91,92] The result is

$$\partial_\tau\mathcal{T}^{\tau\tau} + \frac{1}{\tau}\partial_\eta\mathcal{T}^{\eta\tau} + \partial_v\mathcal{T}^{v\tau} = -\frac{1}{\tau}\mathcal{T}^{\eta\eta} \tag{174}$$

where we defined

$$\mathcal{T}^{ab} = \tau \Lambda^a_\mu \Lambda^b_\nu \, T^{\mu\nu}. \tag{175}$$

and the index $v = x, y$. For the $\tau\eta$ component,

$$\partial_\tau \mathcal{T}^{\tau\eta} + \frac{1}{\tau}\partial_\eta \mathcal{T}^{\eta\eta} + \partial_v \mathcal{T}^{v\eta} = -\frac{1}{\tau}\mathcal{T}^{\eta\tau}. \tag{176}$$

Both $\mathcal{T}^{\tau\tau}$ and $\mathcal{T}^{\tau\eta}$ conservation laws contain the geometrical source term. Transverse momentum conservation is simpler:

$$\partial_\tau \mathcal{T}^{\tau v} + \frac{1}{\tau}\partial_\eta \mathcal{T}^{\eta v} + \partial_w \mathcal{T}^{wv} = 0, \tag{177}$$

where v and w are transverse coordinate indices. When testing one's code for the energy–momentum conservation, the following form may be more convenient:

$$\frac{d}{d\tau}\int dxdyd\eta \, \tilde{T}^{\tau\mu} = 0. \tag{178}$$

The half-transformed $\tilde{T}^{a\mu} = \tau \Lambda^a_\nu \mathcal{T}^{\nu\mu}$ satisfies the conservation law $\partial_\tau \tilde{T}^{\tau\mu} + \tilde{\partial}_\eta \tilde{T}^{\eta\mu} + \partial_v \tilde{T}^{v\mu} = 0$ without the geometrical source terms exactly like Eq. (170).

For the shear and the bulk evolution equations in Eq. (145) or (147), transformation from the Minkowski space to the $\tau - \eta$ coordinate space is straightforward, but it is a lot more involved algebraically. For more details see Refs. 9, 67 and 93.

5.2. *Numerical solution of conservation equations*

In this section, we will first discuss conservation laws in the Minkowski coordinates where the conservation laws are

$$\partial_\mu T^{\mu\nu} = 0, \quad \partial_\mu J^\mu_B = 0. \tag{179}$$

In the Milne coordinate system, the energy–momentum conservation takes a slightly different form

$$\tilde{\partial}_a \mathcal{T}^{ab} = \mathcal{S}^b, \tag{180}$$

where $\mathcal{S}^b$ is the geometric source term in Eqs. (174) and (176). However, as will be shown shortly, the methods illustrated below can be easily adapted to this case.

For vHydro, the energy–momentum tensor is given in a general reference frame by the decomposition

$$T^{\mu\nu} = T^{\mu\nu}_{\rm id} + \pi^{\mu\nu} - \Pi\Delta^{\mu\nu} \tag{181}$$

where

$$T^{\mu\nu}_{\rm id} = \varepsilon u^\mu u^\nu - P(\varepsilon, \rho_B)\Delta^{\mu\nu} \tag{182}$$

is the ideal fluid part of the tensor. The net baryon current has the form $J^\mu_B = \rho_B u^\mu + V^\mu_B$. The equations that need to be solved are given in Eq. (179), together

with the relaxation equations for the dissipative flows, for example the IS equations (147). The first step in solving the hydrodynamic equations is their initialization. Let us assume that some microscopic pre-equilibrium dynamical theory provides us with a baryon current $J^\mu_B(x)$ and energy–momentum tensor $T^{\mu\nu}(x)$ for points x^μ on some Cauchy surface on which we want to initialize the hydrodynamic evolution stage. The following projection steps, to be taken at each point x on that surface, yield the required initial value fields[i]:

First we define the local fluid rest frame by solving the eigenvalue equation $T^\mu_\nu u^\nu = \varepsilon u^\mu$ for its normalized timelike eigenvector u^μ. The associated eigenvalue gives us the LRF energy density ε. The LRF baryon density is obtained from J^μ_B by projecting onto u_μ: $\rho_B = u_\mu J^\mu_B$. The initial heat flow V^μ_B is the component of J^μ_B perpendicular to u^μ: $V^\mu = \Delta^{\mu\nu} J_{B,\nu}$. Now that we know the LRF energy and baryon densities we can compute the LRF pressure P from the equation of state of the fluid, $P(\varepsilon, \rho_B)$. Next, the bulk viscous pressure is obtained from $\Pi = -\frac{1}{3}\Delta_{\mu\nu}T^{\mu\nu} - P$. Finally, the shear stress is obtained as $\pi^{\mu\nu} = T^{\mu\nu} - \varepsilon u^\mu u^\nu + (P + \Pi)\Delta^{\mu\nu}$ or, equivalently, as $\pi^{\mu\nu} = T^{\langle\mu\nu\rangle} \equiv \Delta^{\mu\nu}_{\alpha\beta} T^{\alpha\beta}$.

For a simple illustration of numerical methods that can solve the hydrodynamic equations, let us first consider a single conservation law in one-dimensional. There is no difficult conceptual obstacle in extending this case to the multi-component, multi-dimension cases such as the IS equations. The conservation equation is

$$\partial_t u = -\partial_x j. \tag{183}$$

We need to supplement this equation with a relationship between the density u and the current j. Simplest example is $j = vu$ with a constant speed of propagation v. But in general j is a non-linear function(al) of u. For instance, the ideal part, Eq. (182), is certainly not in this simple form due to the normalization condition $u_0^2 = \sqrt{1 - \mathbf{u}^2}$ and also to the presence of the pressure term. In the dissipative cases, the relaxation equation

$$(\partial_t + 1/\tau_R) j = -(D/\tau_R)\partial_x u \tag{184}$$

determines the relationship between j and u. In such cases, the numerical methods discussed in this section needs to be applied in two steps. In the first step, the conservation laws are used to advance the time component of the currents using the methods that will be discussed here. In the second step, the spatial part of the currents needs to be reconstructed from the time components. The relaxation equations also need to be solved separately, although the techniques discussed here can be easily adapted to handle the relaxation equation as well.

For the simple $j = vu$ case with a constant v, the equation becomes

$$\partial_t u = -v\partial_x u. \tag{185}$$

[i]The following paragraph refers to the vHydro decomposition (10, 181). A slightly modified projection method applies for the aHydro and vaHydro decompositions (150), (151) and (157).[77]

This is an advection equation and has a simple solution

$$u(t,x) = f(x - vt). \tag{186}$$

That is, at any given time, the solution is just the translation of the initial profile by vt. Analytically, this is trivial. However, it is remarkable how difficult it can be to maintain the initial profile in numerical solutions. We will often use this as the simplest test case for our algorithms.

To solve the conservation equation numerically, one first needs to discretize time and space. We define

$$u_i^n = u(t_n, x_i) \tag{187}$$

where $t_n = t_0 + nh$ and $x_i = x_0 + ia$ for any function $u(t,x)$ of time and space. Here h is the time step size and a is the spatial cell size. Physically, it is important to have the following properties in the discretization method. First, the method should conserve total u explicitly, that is, $\sum_i u_i^n = \sum_i u_i^{n+1}$ modulo the boundary terms. For this, one requires that the discretized form of the divergence to take the form

$$(\partial_x j)_i^n \to \frac{j_i(u^n) - j_{i-1}(u^n)}{a} \tag{188}$$

where $j_i(u^n)$ is the discretized representation of the current j at x_i ant t_n. One can easily see that in the sum $\sum_{i=0}^{N}(\partial_x j)_i^n$ only the boundary terms would survive. The details of the boundary terms depend on the method. However, as long as the boundaries are far away from the physical region, the boundary terms should be vanishingly small. If the boundary of the space is not too far away from the physical region, then some suitable discrete boundary conditions should be imposed.

The second requirement is simple, yet quite demanding: If $u_i^0 \geq 0$ for all i, then we would like this property to be maintained for any future time. For instance, if u represents the energy density, then it should never become negative.

To illustrate some of these issues, consider again the advection equation $\partial_t u = -v\partial_x u$ with $v > 0$. Let the initial condition be a rectangle: $u_i^0 = u_c$ for $b \leq i \leq f$ and $u_i^0 = 0$ otherwise. This is a prototype of many situations where two smoothly varying regions are joined by a stiff gradient. The simplest discretization method of $\partial_t u = -v\partial_x u$ is the forward-time centered-space (FTCS) method

$$u_i^{n+1} = u_i^n - \frac{vh}{2a}(u_{i+1}^n - u_{i-1}^n) \tag{189}$$

which is correct up to $O(h^2)$ and $O(a^2)$ errors. Since the second term in the right-hand side is supposed to be a correction, we require $|vh/a| < 1$. This is certainly in the form of Eq. (188) and hence conserves the total u.

According to the analytic solution Eq. (186), the space behind the back edge (x_b) of the rectangle should always have $u^n = 0$. However, according to Eq. (189)

the cell right behind the back edge becomes non-zero and negative after the first time step

$$u_{b-1}^1 = -\frac{vh}{2a}u_c. \tag{190}$$

At the same time, the front edge starts to get distorted by the same amount

$$u_f^1 = u_c - u_{b_1}^1 > u_c. \tag{191}$$

At the next time step, u_{b-1}^2 becomes even more negative

$$u_{b-1}^2 = -\frac{vh}{a}u_c + \left(\frac{vh}{2a}\right)^2 u_c \tag{192}$$

while u_f deviates even more from u_c

$$u_f^2 = u_c - u_{b-1}^2 \tag{193}$$

Furthermore at t_2, the next cell in the empty region becomes non-zero $u_{b-2}^2 = (\frac{vh}{2a})^2 u_c$. Clearly, both the profile preservation and the positivity of the solution are grossly violated by this method even though the total u is conserved. In addition, one can easily see that the growth at x_{b-1} will continue, indicating that this method is unconditionally unstable.

In order to cure the negativity problem, one may note that the trouble above mainly comes from the centered nature of the $O(a^2)$ numerical derivative in Eq. (189). Instead, one may try the first-order approximation[j]

$$u_i^{n+1} = u_i^n - \frac{vh}{a}(u_i^n - u_{i-1}^n) \tag{194}$$

In this "up-wind scheme", u_{b-1}^1 trivially vanishes at t_1. In fact, all u_{b-i} for $i \geq 1$ will remain zero for all times. Similarly, one can show that the numerical solution is positive and bounded everywhere as long as $|vh/a| < 1$. If $v < 0$, mirror-image conclusions can be reached if one uses $(\partial_x u)_i \approx (u_{i+1} - u_i)/a$.

Positivity is thus maintained in this up-wind scheme. However, as the system evolves in time, the shape of the solution gets more and more distorted. This is because the first-order difference

$$(u_i^n - u_{i-1}^n)/a = \partial_x u(t_n, x_i) - \frac{a}{2}\partial_x^2 u(t_n, x_i) + O(a^2) \tag{195}$$

is too crude an approximation of the first-order derivative. The second derivative term in Eq. (195) in fact introduces too much artificial (numerical) damping to preserve the shape for long. In effect, the profile at t is the convolution of the initial profile and the Gaussian Green function of the diffusion equation (Eq. (92)) with the diffusion constant given by $D = \frac{a}{2h}$. As one can see in Eq. (92), the width of the Gaussian grows linearly with time. Hence, the initial profile will be smeared out quickly.

[j]This is in fact trivially exact when $a = vh$ since in that case $u_i^{n+1} = u_{i-1}^n$. That is, the whole profile moves by one spatial cell at each time step. However, this would not work for more general currents.

Better discretization methods must keep the positivity preserving nature of the up-wind method and at the same time must have a better approximation for the spatial derivative than the simple first-order difference for shape preservation. To devise better discretization methods more systematically, consider first dividing the space into $N+1$ cells of size a labeled by integers 0 through N. The ith cell starts at $x_{i-1/2} = x_i - a/2$ and ends at $x_{i+1/2} = x_i + a/2$. (See Fig. 3.) Averaging over one spatial cell and integrating over one time step, the conservation law $\partial_t u = -\partial_x j$ becomes

$$\bar{u}_i^{n+1} = \bar{u}_i^n - \frac{1}{a}\int_{t_n}^{t_{n+1}} dt(j(t, x_{i+1/2}) - j(t, x_{i-1/2})) \tag{196}$$

where $\bar{u}_i^n = \bar{u}_i(t_n)$ is the cell average. This is an exact expression which can be used as the basis for further approximation. This type of methods are known as the finite volume methods.

Approximating the time integral using the midpoint rule, we get

$$\bar{u}_i^{n+1} = \bar{u}_i^n - \frac{h}{a}(j(t_{n+1/2}, x_{i+1/2}) - j(t_{n+1/2}, x_{i-1/2})) + O(h^3) \tag{197}$$

where $t_{n+1/2} = t_n + h/2$. There are few things that should be mentioned here. First, the basic quantities to calculate are the cell-averaged values $\bar{u}_i^n$. Second, we need to approximate the function $u(t,x)$ itself from $\bar{u}_i^n$ because the right hand side contains $u(t,x)$ evaluated at $t_{n+1/2}$ and $x_{i\pm1/2}$. An approximate form of $u(t_n, x)$ is also needed for obtaining $\bar{u}_i^{n+1}$ for the next time step (see below). Therefore, how we approximate $u(t,x)$ and evaluate $j_{i\pm1/2}^{n+1}$ determine different numerical schemes and the accuracy of the given scheme.

In many schemes, the values at spatial half points are not unique because the interpolating function approximating $u(t,x)$ is usually only piece-wise continuous. For instance, see Figs. 3 and 4. One way to deal with the ambiguity in evaluating

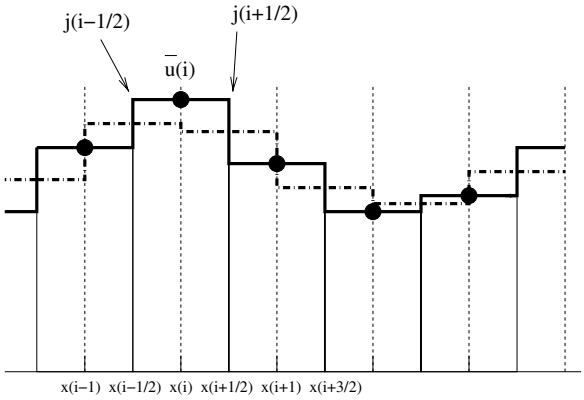

Fig. 3. Spatial grid used in deriving finite volume methods. The solid line is the lowest order histogram function approximation of $u(t,x)$ in the x_i-centered grid. The dot–dash line is the projection of the x_i-centered grid onto the $x_{i+1/2}$-centered grid.

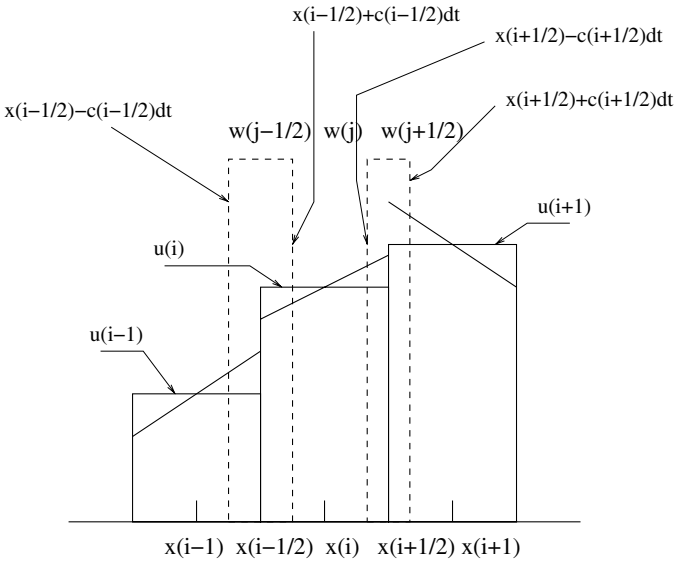

Fig. 4. A schematic view of the cell division used in the Kurganov–Tadmor scheme.

$j(t_{n+1/2}, x_{i\pm1/2})$ is to just avoid evaluating it at the boundaries. The staggered nature of the space and time indices in Eq. (197) suggests an obvious way to do so. Suppose that the initial data is given for $\bar{u}_i^n$ where the ith grid is centered at x_i and has the spatial interval $[x_{i-1/2}, x_{i+1/2}]$. For the next time step, instead of updating the values of $\bar{u}_i$ within the intervals $[x_{i-1/2}, x_{i+1/2}]$, we update the values of $\bar{u}_{i+1/2}$ within the shifted intervals $[x_i, x_{i+1}]$. Using the lowest order approximation for $u(t, x)$ (the histogram functions in Fig. 3), this yields

$$\bar{u}_{i+1/2}^{n+1} = \frac{\bar{u}_{i+1}^n + \bar{u}_i^n}{2} - \frac{h}{a}(j(u_{i+1}^{n+1/2}) - j(u_i^{n+1/2})) \tag{198}$$

where $(\bar{u}_i^n + \bar{u}_{i+1}^n)/2$ is the average value of $u(t_n, x)$ in the shifted interval $[x_i, x_{i+1}]$ using the histogram function in Fig. 3. For the values of $u_{i+1}^{n+1/2}$ at $t_{n+1/2}$, the forward Euler method

$$u_i^{n+1/2} = \bar{u}_i^n - \frac{h}{2}(\partial_x j)_i^n + O(h^2) \tag{199}$$

is enough since the overall error in the midpoint rule is $O(h^3)$. In this way, we avoid evaluating the current at the cell boundaries. For the next time step, we shift back to the original grid. This staggered method is a slightly generalized form of the Lax–Friedrichs scheme which is second-order accurate in space and third order accurate in time. The original Lax–Friedrichs scheme is only second-order in time because the currents are evaluated at t_n instead of at $t_{n+1/2}$.

Equation (199) involves evaluating numerical derivative of the current j at x_i. This cannot be exactly determined when all one has is data on the average values $\bar{u}_i^n$. For instance, $(j_x)_i^n$ could be the first-order approximations $(j_{i+1}^n - j_i^n)/a$ or

$(j_i^n - j_{i-1}^n)/a$, or the second-order approximation $(j_{i+1}^n - j_{i-1}^n)/2a$, or any other approximate form. In normal situations, choosing a higher order formula should be better than the first-order ones. But this is not always the case when the gradient is stiff.

We have already shown that using the central difference $(j_{i+1}^n - j_{i-1}^n)/2a$ in the forward Euler method (the FTCS method in Eq. (189)) can be disastrous when the gradient is stiff, although it can be safely (and preferably) used in smooth regions. When gradient is stiff, one should instead use the up-wind method Eq. (194) to maintain the positivity. Therefore, an intelligent scheme would choose the derivative according to some approximate measure of the true gradient. One way to do this is to choose the gradient according to the following scheme:

$$(\partial_x u)_i^n = \begin{cases} 0 \text{ if } \bar{u}_i^n < \bar{u}_{i\pm1}^n \text{ or } \bar{u}_i^n > \bar{u}_{i\pm1}^n \\ \text{else } \operatorname{sign}(\bar{u}_{i+1}^n - \bar{u}_i^n) \min\left(\theta\dfrac{|\bar{u}_{i+1}^n - \bar{u}_i^n|}{a}, \dfrac{|\bar{u}_{i+1}^n - \bar{u}_{i-1}^n|}{2}, \theta\dfrac{|\bar{u}_i^n - \bar{u}_{i-1}^n|}{a}\right). \end{cases} \tag{200}$$

The first line indicates that the function has either a maximum or a minimum within the interval. Therefore the slope at x_i can be best approximated by 0. The second line applies when the function is changing monotonically near x_i. The parameter $1 \le \theta < 2$ is there to be slightly more general. This choice of the derivative is called the "generalized minmod flux limiter".

The Lax–Friedrichs scheme represented by Eq. (198) is only $O(a^2)$ accurate because we have used the histogram function as an approximation for $u(t_n, x)$. Needless to say, this is the lowest order approximation. As a result, the Lax–Friedrichs scheme contains too much numerical diffusion to be practically useful. Both of these facts can be easily seen from the Taylor expansion

$$\frac{\bar{u}_i^n + \bar{u}_{i+1}^n}{2} = \bar{u}_{i+1/2}^n + \frac{a^2}{8}\partial_x^2 u_{i+1/2}^n + O(a^4) \tag{201}$$

where the second derivative term is the $O(a^2)$ error term that also causes strong diffusion. In time, this diffusion distorts the solution too much just as in the first-order up-wind method.

To obtain a better approximation, one needs to evaluate $u(t, x)$ more accurately using the average values from the nearest neighbor cells. If one uses the linear interpolant (see Fig. 4)

$$\hat{u}_i^n(x) = \bar{u}_i^n + (\partial_x u)_i^n (x - x_i) \tag{202}$$

for each interval $[x_{i-1/2}, x_{i+1/2}]$, then the scheme should become at least $O(a^3)$. Using this to improve the estimate of $\bar{u}_{i+1/2}^n$ adds a correction term to the lowest-order result Eq. (198)

$$\bar{u}_{i+1/2}^{n+1} = \frac{\bar{u}_i^n + \bar{u}_{i+1}^n}{2} - \frac{h}{a}(j(t_{n+1/2}, x_{i+1}) - j(t_{n+1/2}, x_i)) - \frac{a}{8}((\partial_x u)_{i+1}^n - (\partial_x u)_i^n). \tag{203}$$

This staggered approach is the second-order NT (Nessyahu–Tadmor) scheme and works reasonably well.[94] The last term on the right-hand side of Eq. (203) cancels the second derivative term in Eq. (201) so that together they represent $\bar{u}^n_{i+1/2}$ with the $O(a^4)$ error. In other words, the last term in Eq. (203) is the anti-diffusion term that is correcting the large second-order diffusion introduced by the symmetric combination $(\bar{u}^n_i + \bar{u}^n_{i+1})/2$. Therefore, this scheme is $O(a^4)$ in the smooth region.

Why don't we then just replace these terms with $\bar{u}^n_{i+1/2}$? If one does that, it just becomes the FTCS scheme in Eq. (189). The difference, the $O(a^4\partial^4_x u(x))$ term, provides just enough numerical diffusion so that spurious oscillations do not propagate from the stiff gradient.

The second-order NT algorithm represented by Eq. (203) is related to another often-used finite element method called the SHASTA algorithm. We start with Eq. (203) but replace

$$\frac{\bar{u}^n_i + \bar{u}^b_{i+1}}{2} \approx \bar{u}^n_{i+1/2} + \frac{1}{8}(u_{i+1} - 2u_{i+1/2} + u_i) + O(a^4) \tag{204}$$

so that

$$\begin{aligned}\bar{u}^{n+1}_{i+1/2} = \bar{u}^n_{i+1/2} - \frac{h}{a}(j(t_{n+1/2}, x_{i+1}) - j(t_{n+1/2}, x_i)) \\ + \frac{1}{8}(\bar{u}^n_{i+1} - 2\bar{u}^n_{i+1/2} + \bar{u}^n_i) - \frac{a}{8}((\partial_x u)^n_{i+1} - (\partial_x u)^n_i).\end{aligned} \tag{205}$$

At this point, this is no longer a finite volume method even though we will keep using the notation $\bar{u}^n_i$ to represent the value of u at t_n and x_i. It is also not a staggered method any more as the right-hand side contains $\bar{u}^n_{i+1/2}$. Re-labeling the spaces indices $i + 1/2 \to i$ and $i \to i - 1$ so that the new grid size is $a' = a/2$, we get

$$\begin{aligned}\bar{u}^{n+1}_i = \bar{u}^n_i - \frac{h}{2a}(j(t_{n+1/2}, x_{i+1}) - j(t_{n+1/2}, x_{i-1})) \\ + \frac{1}{8}(\bar{u}^n_{i+1} - 2\bar{u}^n_i + \bar{u}^n_{i-1}) - \frac{a}{16}((\partial_x u)^n_{i+1} - (\partial_x u)^n_{i-1})\end{aligned} \tag{206}$$

with the appropriate scaling of the derivatives in the last term and after renaming $a' \to a$. With $u(t_{n+1/2}, x_{i\pm1})$ given by Eqs. (199) and (206) represents the basic SHASTA algorithm.

In practice, Eq. (206) is broken up into two stages to ensure positivity. Specifying $j = vu$, the first transport step is[k]

$$\begin{aligned}w^{n+1}_i = \bar{u}^n_i + \frac{1}{8}(\bar{u}^n_{i+1} - 2\bar{u}^n_i + \bar{u}^n_{i-1}) \\ - \frac{vh}{2a}\left(\bar{u}^n_{i+1} - \frac{vh}{2}(\partial_x u)^n_{i+1} - \bar{u}^n_{i-1} + \frac{vh}{2}(\partial_x u)^n_{i-1}\right)\end{aligned} \tag{207}$$

[k]In the original SHASTA algorithm, $(\bar{u}^n_{i+1} - 2\bar{u}^n_i + \bar{u}^n_{i-1})$ is used in place of $((\partial_x u)^n_{i+1} - (\partial_x u)^n_{i-1})/2$ in this stage. In practice, as long as $|vh/a|$ is small, this difference does not matter much. But it is crucial that a flux limiter is used in the second anti-diffusion step.

again using Eq. (199). If $\bar{u}_l^n \geq 0$ for all l, then as long as $|vh/a| < 1/4$, w_i^{n+1} is positive.

The second stage is the anti-diffusion step

$$\bar{u}_i^{n+1} = w_i^{n+1} - \frac{a^2}{8}(\partial_x^2 w)_i^{n+1} \tag{208}$$

where $(\partial_x^2 w)_i^{n+1}$ represents numerical estimate of the second derivative at x_i that preserves the positivity. The numerical approximation suggested by the last term in Eq. (206) turned out not to preserve the positivity. The original formulation of the SHASTA algorithm by Boris and Book uses a conservative form

$$(\partial_x^2 w)_i^{n+1} = \frac{1}{a}((w_x)_{i+1}^{n+1} - (w_x)_i^{n+1}) \tag{209}$$

where

$$(w_x)_{i+1}^{n+1} = \begin{cases} 0 \text{ if } \Delta_i^{n+1}, \Delta_{i+1}^{n+1} \text{ and } \Delta_{i+2}^{n+1} \text{ do not all have the same sign.} \\ \text{else } \operatorname{sign}(\Delta_{i+1}^{n+1}) \min(8|\Delta_i^{n+1}|, |\Delta_{i+1}^{n+1}|, 8|\Delta_{i+2}^{n+1}|) \end{cases} \tag{210}$$

with

$$\Delta_{i+1}^{n+1} = (w_{i+1}^{n+1} - w_i^{n+1})/a. \tag{211}$$

This is similar to the minmod flux limiter and maintains the positivity. The SHASTA algorithm is used in many hydrodynamics simulation programs for ultra-relativistic heavy ion collisions[95] including pioneering works in Refs. 96, 91 and also later works in Refs. 67, 97–101.

The second-order NT scheme and the SHASTA scheme in practice work fairly well.[102] However, in these schemes the $h \to 0$ limit cannot be taken since the numerical viscosity behaves like $\sim 1/h$. It would be convenient to be able to take this limit because one can then formulate the discretized problem as a system of coupled ordinary differential equations in time. Many techniques for the ordinary differential equations such as the Runge–Kutta methods then become available to control the accuracy of the time evolution. So far different time integration techniques were not available other than the midpoint rule in Eq. (197).

One way to achieve this is to subdivide the cells as shown in Fig. 4 with the piecewise linear approximation for $u(t, x)$. The size of the cell containing the discontinuity at the half integer point $x_{i+1/2}$ is controlled by the local propagation speed $c_{i+1/2}$. That is, the subcell surrounding $x_{i+1/2}$ is between the left boundary $x_{i+1/2}^l = x_{i+1/2} - c_{i+1/2}h$ and the right boundary $x_{i+1/2}^r = x_{i+1/2} + c_{i+1/2}h$. Then the cells containing the boundaries and the cells not containing the boundaries (between $x_{i-1/2}^r$ to $x_{i+1/2}^l$) are independently evolved. For the subcell containing $x_{i+1/2}$

$$w_{i+1/2}^{n+1} = \frac{\bar{u}_{i+1/2}^l + \bar{u}_{i+1/2}^r}{2} - \frac{1}{2c_{i+1/2}}(j(\bar{u}_{i+1/2}^r) - j(\bar{u}_{i+1/2}^l)) + O(h) \tag{212}$$

which is basically Eq. (198). Here the superscripts r and l means the value of the approximate $u(t_n, x)$ at the boundary points $x_{i+1/2}^r$ and $x_{i+1/2}^l$, respectively. Within

the smooth region between $x^r_{i-1/2}$ and $x^l_{i+1/2}$, we get using Eq. (197)

$$w_i^{n+1} = \frac{\bar{u}^l_{i+1/2} + \bar{u}^r_{i-1/2}}{2} - \frac{h}{a}(j(\bar{u}^l_{i+1/2}) - j(\bar{u}^r_{i-1/2})) + O(h^2) \tag{213}$$

where the first term on the right-hand side is obtained by applying the trapezoid rule. The divided cells are then projected onto the original grid using the size of the cells as the weight to get

$$\bar{u}_i^{n+1} = \frac{c_{i-1/2}h}{a} w^{n+1}_{i-1/2} + \frac{c_{i+1/2}h}{a} w^{n+1}_{i+1/2} + \left(1 - \frac{(c_{i-1/2} + c_{i+1/2})h}{a}\right) w_i^{n+1}. \tag{214}$$

When the $h \to 0$ limit is taken, this procedure yields

$$\frac{d\bar{u}_i}{dt} = -\frac{H_{i+1/2} - H_{i-1/2}}{a} \tag{215}$$

where

$$H_{i+1/2} = \frac{j(\bar{u}^+_{i+1/2}) + j(\bar{u}^-_{i+1/2})}{2} - c_{i+1/2}\frac{\bar{u}^+_{i+1/2} - \bar{u}^-_{i+1/2}}{2} \tag{216}$$

where now $\bar{u}^+_{i+1/2}$ and $\bar{u}^-_{i+1/2}$ are the values of the piece-wise linear $u(t,x)$ when approaching $x_{i+1/2}$ from the right and from the left, respectively. They are given by

$$\bar{u}^+_{i+1/2} = \bar{u}_{i+1} - (a/2)(\partial_x u)_{i+1}, \tag{217}$$

$$\bar{u}^-_{i+1/2} = \bar{u}_i + (a/2)(\partial_x u)_i \tag{218}$$

again using the minmod flux limiter for the derivatives. This is known as the second-order Kurganov–Tadmor (KT) scheme[103] and it is implemented in the (3+1)-dimensional event-by-event viscous hydrodynamics simulation program MUSIC.[9,92] The numerical viscosity in the smooth regions is known to be $O(a^3\partial_x^4 u)$.

The structure of the KT algorithm, Eqs. (215) and (216), is the same for the lowest-order, second-order and the third-order algorithms. All one needs to do to improve accuracy is to get a better estimate of $\bar{u}^\pm_{i+1/2}$. Actually, it is instructive to consider the lowest-order result which uses the histogram function as the approximation of $u(x)$. One then has $\bar{u}^+_{i+1/2} = \bar{u}_{i+1}$ and $\bar{u}^-_{i+1/2} = \bar{u}_i$. It is easy to see in this case that if $j = vu$ and hence $c_{i+1/2} = |v|$, Eq. (215) automatically becomes the up-wind method.

We now have a set of ODE's. What is a good choice of the ODE solver? One of the physical requirement is again the positivity. For instance, suppose u represents particle density. One knows that u can never be negative. One of the schemes that preserves the positivity is the Heun's method which is one of the second-order Runge–Kutta schemes. The equation $du/dt = f$ is numerically solved by following

these steps:

$$\bar{u}_j^* = \bar{u}_j^n + hf(t_n, \bar{u}^n), \tag{219}$$

$$\bar{u}_j^{**} = \bar{u}_j^* + hf(t_{n+1}, \bar{u}^*), \tag{220}$$

$$\bar{u}_j^{n+1} = \frac{1}{2}(u_j^n + u_j^{**}). \tag{221}$$

Positivity is maintained at each stage with a suitable choice of the flux limiter such as the minmod flux limiter.

For 3-dimensional (and similarly for 2-dimensional), a simple extension

$$\frac{d}{dt}\bar{u}_{ijk} = -\frac{H^x_{i+1/2,j,k} - H^x_{i-1/2,j,k}}{a_x} - \frac{H^y_{i,j+1/2,k} - H^x_{i,j-1/2,k}}{a_y} - \frac{H^z_{i,j,k+1/2} - H^z_{i,j,k-1/2}}{a_z} \tag{222}$$

works well. In curvilinear coordinate systems such as the Milne coordinates, one may not have the conservation law in the form $\partial_\mu J^\mu = 0$. Instead, it may take the form

$$\partial_a J^a = S \tag{223}$$

where S is the geometrical source term that does not involve derivatives. The KT algorithm can be easily adapted to this case by simply adding the source term on the right-hand side. Namely,

$$\frac{d\bar{u}_i}{dt} = -\frac{H_{i+1/2} - H_{i-1/2}}{a} + S(\bar{u}_i). \tag{224}$$

In implementing the KT scheme, one needs the maximum speed of propagation at $x_{i\pm1/2}$. If there is only one variable u and one current j, then the speed of propagation in the ith direction is

$$c_i = \left|\frac{\partial j_i}{\partial u}\right|. \tag{225}$$

If there are more than one current, then we first define the Jacobian matrix

$$J_i^{ab} = \frac{\partial j_i^a}{\partial u_b} \tag{226}$$

where $i = 1, 2, 3$ is the space index and $a = 1, \ldots, M$ labels the conserved quantities. Therefore we have 3 $M \times M$ matrices. The maximum propagation speed in the ith direction is

$$c_i = \max(|\lambda_1|, \ldots, |\lambda_M|) \tag{227}$$

where λ's are the eigenvalues of the Jacobian J_i^{ab}. When discretizing in time, the original authors of the KT algorithm recommended the time step h to be small enough so that $|\max(c_i)h/a| < 1/8$.

For the explicit form of the c_i for the (3+1)-dimensional ideal hydrodynamics including the net baryon currently used in MUSIC, see Ref. 92. For implementation of the event-by-event (3+1)-dimensional viscous hydrodynamics in MUSIC, see Refs. 9 and 58. Additional valuable information on the algorithms used in solving the VHYDRO equations can be found in Ref. 104. For some comparisons of various schemes discussed in the section, see Ref. 102.

There are many other numerical schemes that are currently in use but we unfortunately did not have space to discuss. These include, but not limited to, a PPM (Piece-wise Parabolic Method) scheme,[105] a Lagrangian scheme where the grid points follow the movement of fluid cells,[106] Riemann solvers,[102,107] and a SPH (smoothed particle hydrodynamics) method.[108] The simple FTCS scheme has also been employed for the viscous hydrodynamics[109,110] for smooth initial conditions.

5.3. *Freeze-out hypersurface and Cooper–Frye formula for particle production*

When a hydrodynamic system is expanding, there comes a time when the system is too dilute to be treated with hydrodynamics (c.f. Sec. 4.1). From this point on, the system is basically a collection of non-interacting particles. In realistic systems, this time is not the same for all fluid cells. As the system starts to expand at τ_0, there are cells at the periphery of the system that are dilute enough to "freezes out" in a very short time. As time elapses, expansion of the system can cause hot and dense matter to flow into the location of those frozen cells. These will eventually freeze-out, too. Therefore, the freeze-out surface volume cannot be a simple 3-dimensional volume. It is a complicated 3-dimensional volume in the 4-dimensional space-time.

To illustrate this point, consider the following Gubser solution of the boost-invariant and azimuthally symmetric ideal-hydrodynamics[85 1]:

$$T(\tau, r) = \frac{2T_0}{(2q\tau[1 + 2q^2(\tau^2 + r^2) + q^4(\tau^2 - r^2)^2])^{1/3}} \tag{228}$$

where $r^2 = x^2 + y^2$ and $\tau = \sqrt{t^2 - z^2}$. It is a simple matter of taking the τ derivative of $T(\tau, r)$ to see that for $r > r_0$ where $r_0 = \frac{3+\sqrt{5}}{2q}$, there are two values of τ where $\partial_\tau T$ vanishes. Since $\partial_\tau T$ is negative for small τ, this means that $T(\tau, r)$ at fixed $r > r_0$ will have a minimum and then a maximum. This is illustrated in the left panel in Fig. 5. The solid line is for $qr = 1$ which is near the center of the system. The temperature at that position decreases monotonically. At $r = r_0$, there is an inflection point but the behavior is till monotonic. In the $qr = 5$ case, one can clearly see that the temperature decreases at first but a some point it starts to rise again as the pressure pushes hot matter from the central region towards the periphery of the system. Assuming that the freeze-out temperature is between the minimum and the maximum of T/T_0, the position $qr = 5$ will contribute to the final particle spectrum (freeze-out) three times.

[1]Analytic solutions of the ideal hydrodynamics do exist for special cases, but not for general cases.

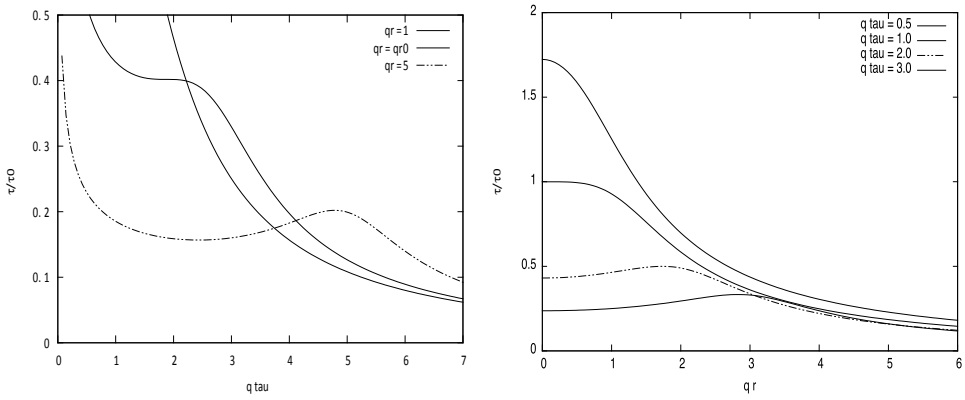

Fig. 5. Plot of $T(\tau, r)/T_0$ for the Gubser solution. Here $qr_0 = (3 + \sqrt{5})/2$. The left panel shows $T(\tau, r)/T_0$ at fixed r's and the right panel shows $T(\tau, r)$ at fixed τ's.

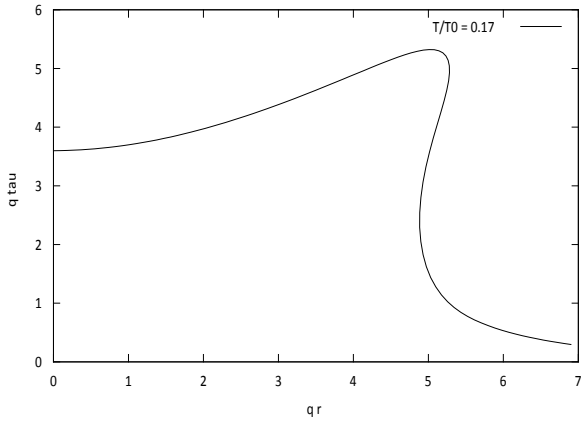

Fig. 6. Plot of the hypersurface with $T(\tau, r)/T_0 = 0.17$ for the Gubser solution.

The plot of isothermal curve with $T(\tau, r)/T_0 = 0.17$ is shown in Fig. 6. One may think of this as representing the "freeze-out" hypersurface in the Gubser solution. The long tail that can be seen above $qr \gtrsim 5$ is unrealistic. In more realistic simulations, the simulation starts at times above the long tail. Nevertheless, the Gubser solution contains much of the features that the more realistic numerical solutions exhibit.[9,111–113]

At the freeze-out hypersurface, the fluid is to be converted to particles according to the local equilibrium condition. In the kinetic theory, the particle number current for the ith particle is given by

$$j_i^\mu(x) = g_i \int \frac{d^3p}{(2\pi)^3 p^0} \, f_i(x, p) \, p^\mu \tag{229}$$

where $f_i(x,p)$ is the phase space density and g_i is the degeneracy. The number of ith particle in a 3-dimensional hypersurface is then given by

$$\int d\sigma_\mu j_i^\mu(x) = g_i \int \frac{d^3p}{(2\pi)^3 p^0} \int d\sigma_\mu \, p^\mu f_i(x,p) \tag{230}$$

where $d\sigma_\mu$ is the hypersurface element. Hence, the momentum spectrum is

$$E_p \frac{dN_i}{d^3p} = \frac{g_i}{(2\pi)^3} \int d\sigma_\mu \, p^\mu f_i(x,p). \tag{231}$$

This is the celebrated Cooper–Frye formula.[114]

Hydrodynamics deals with the energy density and its flow. Experiments measure the momentum distribution of identified particles. Cooper–Frye formula provides the link between them. In ideal hydrodynamics, local equilibrium is strictly maintained. Hence once we find the freeze-out hypersurface (equivalently the energy density via the equation of state), all one has to do is to integrate Eq. (231) over the freeze-out hypersurface with $f_i(x,p) = 1/(e^{(p^\mu u_\mu - \mu_B)/T_{\rm FO}} + a_i)$ where $T_{\rm FO}$ is the freeze-out temperature, $a_i = -1$ for bosonic statistics, $a_i = 1$ for fermionic statistics, and $a_i = 0$ for classical (Boltzmann) statistics.

The freeze-out surface we need to integrate over has the shape shown in Fig. 6 which requires a closer inspection. Suppose all parts of the system reaches the freeze-out temperature at the same Minkowski time $t_{\rm FO}$ and only once. In that case, the freeze-out hypersurface is just the Minkowski spatial volume. The integration element is just then $d\sigma_0 = dxdydz$. All other components vanish. This is simple, but not a realistic scenario in relativistic heavy ion collisions as explained in the previous section.

In the Milne coordinate system, the volume elements in each direction are given by

$$d\sigma_a = (\tau dxdyd\eta, -\tau d\tau dyd\eta, -\tau d\tau dxd\eta, -\tau d\tau dxdy). \tag{232}$$

When the freeze-out hypersurface is specified by the freeze-out proper time $\tau_f(x,y,\eta)$, the surface element on this surface is obtained by replacing $d\tau$ in Eq. (232) with $(\partial\tau_f/\partial x_i)dx_i$:

$$d\sigma_a^f = \left(1, -\frac{\partial\tau_f}{\partial x}, -\frac{\partial\tau_f}{\partial y}, -\frac{\partial\tau_f}{\partial\eta}\right) \tau_f dxdyd\eta. \tag{233}$$

If $d\sigma_a^f$ is time-like, then it is guaranteed that $p^a d\sigma_a^f > 0$. Therefore, Eq. (231) has a well defined interpretation that the particles are flowing out of the hypersurface. If $d\sigma_a^f$ is space-like, then depending on the direction of p^a, $p^a d\sigma_a^f$ could be either positive or negative. Equivalently, particles can be flowing into or out of the hypersurface.

Before we discuss the physical situation when this can happen, first we define the dynamic rapidity $y = \tanh^{-1}(p_z/E)$ so that

$$E = m_T \cosh y, \tag{234}$$

$$p^z = m_T \sinh y \tag{235}$$

with $m_T = \sqrt{m^2 + \mathbf{p}_T^2}$. The Milne space momentum is

$$p^a = (m_T \cosh(y - \eta), \mathbf{p}_T, m_T \sinh(y - \eta)/\tau) \tag{236}$$

which is equivalent to using $\Lambda^a_\mu p^\mu$ from (cf. Eq. (166)) but with an extra factor of $1/\tau$ for the η component to conform with the geometrical definition of the hypersurface element Eq. (233).

To illustrate what happens when $d\sigma^f_a$ is space-like, let us consider the Gubser solution again. In this case, $\tau_f(r)$ is a function of the transverse radius $r = \sqrt{x^2 + y^2}$ only. Since the system is boost-invariant, we can also set $\eta = 0$ without loss of generality. The inner product of the momentum and the volume element is

$$p^a d\sigma^f_a = (m_T \cosh y - (\mathbf{p}_T \cdot \hat{\mathbf{r}})\partial_r \tau_f)\tau_f dx dy d\eta \tag{237}$$

where $\hat{\mathbf{r}}$ is the unit vector in the transverse direction. This can become negative if $\partial\tau_f/\partial r > (m_T/p_T)\cosh y > 1$. From Figs. 5 and 6, one can see that large positive gradient $\partial\tau_f/\partial r$ exists in the region where the temperature reaches $T_{\rm FO}$ the second time. At this time, the temperature is going *up* from the minimum in the left panel of Fig. 5. Therefore, this part of the τ_f is not about the fluid freezing-out. It is rather colder matter being heated up to become the a part of the fluid again.

Before one could use the Cooper–Frye formula, one needs to know the freeze-out hypersurface. This is not a trivial problem because hydrodynamic simulations only provide the freeze-out *space-time points.* The freeze-out hypersurface needs to be reconstructed from these points. In $2 + 1$d, this is not so complicated. But in $3 + 1$-dimensional, it can become very involved. Discussion of this important topic however is beyond the scope of this review. An interested reader should consult Ref. 115.

How do we use the Cooper–Frye formula Eq. (231)? If hydrodynamics is not coupled to the hadronic cascade after-burner, then usually the hypersurface integral in Eq. (231) is performed as it is after the hypersurface is reconstructed. The rationale behind it is that when the cell crosses the freeze-out boundary 3 times, the contributions from the first two times should largely cancel each other. This is physically sound because when the fluid cell crosses the freeze-out surface the second time, the particles that are being heated up again are the remnants of the first crossing. When coupling to the hadronic after-burner, an additional condition such as $p^a d\sigma^f_a > 0$ is usually employed.[115–118]

The presence of non-zero shear tensor $\pi^{\mu\nu}$ and the bulk pressure Π signals non-equilibrium. In this case, the Cooper–Frye formula needs to be modified to take

into account the non-equilibrium phase space density. Let

$$f(x,p) = f_{\rm eq}(x,p) + \delta f(x,p). \tag{238}$$

Then the consistency between the hydrodynamic $T^{\mu\nu}$ and the kinetic theory $T^{\mu\nu}_{\rm Kin} = \int \frac{d^3p}{(2\pi)^3 p^0} p^\mu p^\nu f$ requires

$$\pi^{\mu\nu} = \int \frac{d^3p}{(2\pi)^3 p^0}\, p^{\langle\mu} p^{\nu\rangle}\, \delta f(x,p) \tag{239}$$

and

$$\Pi = -\frac{m^2}{3} \int \frac{d^3p}{(2\pi)^3 p^0}\, \delta f(x,p) \tag{240}$$

with

$$p^{\langle\mu} p^{\nu\rangle} = \Delta^{\mu\nu}_{\alpha\beta} p^\alpha p^\beta. \tag{241}$$

These conditions can be satisfied by

$$\begin{aligned}\delta f(x,p) = {} & (A(\bar{E}_p)\Pi(x,p) \\ & + B(\bar{E}_p) p^{\langle\mu} p^{\nu\rangle} \pi_{\mu\nu}(x,p) + \cdots) f_{\rm eq}(x,p)(1 + a_i f_{\rm eq}(x,p))\end{aligned} \tag{242}$$

where again $\bar{E}_p = p^\mu u_\mu$ is the energy in the local rest frame. Here $A(\bar{E}_p)$ and $B(\bar{E}_p)$ must be consistent with Eqs. (239) and (240), but otherwise arbitrary at this point. In the presence of the net-baryon current Eq. (242) also includes $C(\bar{E}_p) p^{\langle\mu\rangle} q_\mu$ with the constraint on $C(\bar{E}_p)$ given by Eq. (138). Exact forms of $A(\bar{E}_p)$ and $B(\bar{E}_p)$ (and $C(\bar{E}_p)$) depend on the form of the scattering cross-sections in the underlying microscopic system. In Ref. 119, it is argued that for most theories, the $\bar{E}_p$ dependence of A and B should be between 1 and $1/\bar{E}_p$. See also Refs. 120 and 121. In most simulations, the constant ansatz is used.

6. Summary

In this review, we have tried to deliver a more general and pedagogic view of the relativistic hydrodynamics currently used in the study of ultra-relativistic heavy ion collisions. One message we tried to convey to the reader was that hydrodynamics is a very general framework and yet it can describe a vast set of complex phenomena. Especially in QGP studies, hydrodynamics is an indispensable tool that connects the QGP properties to the actual observables.

Another message we tried to convey was that the theory of hydrodynamics is a fascinating subject by itself. As discussed in Secs. 3 and 4, there are still many unsolved problems such as finding Kubo formulas for the second-order transport coefficients and finding the right anisotropic equation of state. In view of the apparent collectivity in the high-multiplicity proton–proton and proton–nucleus collisions at the LHC, the theory of collective motion in small systems is also in urgent need of development. In these systems, thermal fluctuations during the hydrodynamic

evolution may not be completely ignored.[122–126] We hope that this review has provided interested readers enough starting points to pursue these and other interesting topics on their own.

In any short review, omission of some important subjects inevitably occurs due to the lack of space. One notable omission in this review is the discussion of the initial state models. As briefly discussed in Sec. 5.2, the initial condition of the hydrodynamic evolution must be given outside of the theory of hydrodynamics. For a meaningful comparison with the experimental data, having the right initial condition including the right energy–momentum fluctuation spectra is crucial. Unfortunately, it is outside the scope of this review and must be left as the subject of a future review.

Acknowledgments

S.J. thanks C. Gale and G. Denicol for many discussions on finer points of hydrodynamics and L.G. Yaffe for generous permission to use some materials from his unpublished note. S.J. is supported in part by the Natural Sciences and Engineering Research Council of Canada. U.H. acknowledges support by the U.S. Department of Energy, Office of Science, Office of Nuclear Physics under Awards No. DE-SC0004286 and (within the framework of the JET Collaboration) DE-SC0004104.

References

1. L. Landau, *Izv. Akad. Nauk Ser. Fiz.* **17** (1953) 51–64.
2. P. F. Kolb and U. W. Heinz, Hydrodynamic description of ultrarelativistic heavy ion collisions. (2003). Published in Quark gluon plasma 3, 634–714. R. Wha and X.-N. Wang (eds.), World Scientific, 2004.
3. P. Huovinen, Hydrodynamical description of collective flow. Chapter 1. (2003).
4. C. Gale, S. Jeon and B. Schenke, *Int. J. Mod. Phys. A* **28** (2013) 1340011.
5. F. Karsch, *Nucl. Phys. A* **698** (2002) 199–208.
6. P. Kovtun, D. T. Son and A. O. Starinets, *Phys. Rev. Lett.* **94** (2005) 111601.
7. H. Song and U. W. Heinz, *Phys. Lett. B* **658** (2008) 279–283.
8. H. Song and U. W. Heinz, *J. Phys. G* **36** (2009) 064033.
9. B. Schenke, S. Jeon and C. Gale, *Phys. Rev. Lett.* **106** (2011) 042301.
10. B. Schenke, S. Jeon and C. Gale, *Phys. Lett. B* **702** (2011) 59–63.
11. H. Song, S. A. Bass and U. Heinz, *Phys. Rev. C* **83** (2011) 054912.
12. H. Petersen, *Phys. Rev. C* **84** (2011) 034912.
13. C. Shen, U. Heinz, P. Huovinen and H. Song, *Phys. Rev. C* **84** (2011) 044903.
14. G. Aad *et al.*, *Phys. Rev. Lett.* **110**(18) (2013) 182302.
15. S. Chatrchyan *et al.*, *Phys. Lett. B* **718** (2013) 795–814.
16. B. Abelev *et al.*, *Phys. Lett. B* **719** (2013) 29–41.
17. A. Adare *et al.*, *Phys. Rev. Lett.* **111**(21) (2013) 212301.
18. I. Kozlov, M. Luzum, G. Denicol, S. Jeon and C. Gale, *Nucl. Phys. A* **931** (2014) 1045.
19. J. Kapusta and C. Gale, *Finite-Temperature Field Theory: Principles and Applications* (Cambridge University Press, 2006).

20. D. Forster, *Hydrodynamic Fluctuations, Broken Symmetry, and Correlation Functions*. Frontiers in Physics: A Lecture Note and Reprint Series (W. A. Benjamin, Advanced Book Program, 1975).
21. L. P. Kadanoff and P. C. Martin, *Annals Phys.* **24** (1963) 419–469.
22. C. P. Herzog, *J. Phys. A* **42** (2009) 343001.
23. P. Kovtun, *J. Phys. A* **45** (2012) 473001.
24. S. Deser and D. Boulware, *J. Math. Phys.* **8** (1967) 1468.
25. R. Baier, P. Romatschke, D. T. Son, A. O. Starinets and M. A. Stephanov, *JHEP* **0804** (2008) 100.
26. G. D. Moore and K. A. Sohrabi, *Phys. Rev. Lett.* **106** (2011) 122302.
27. W. Israel and J. Stewart, *Annals Phys.* **118** (1979) 341–372.
28. G. Denicol, T. Kodama, T. Koide and P. Mota, *J. Phys. G* **35** (2008) 115102.
29. S. Pu, T. Koide and D. H. Rischke, *Phys. Rev. D* **81** (2010) 114039.
30. P. B. Arnold, G. D. Moore and L. G. Yaffe, *JHEP* **0111** (2001) 057.
31. P. B. Arnold, G. D. Moore and L. G. Yaffe, *JHEP* **0305** (2003) 051.
32. P. B. Arnold, C. Dogan and G. D. Moore, *Phys. Rev. D* **74** (2006) 085021.
33. D. Gross and F. Wilczek, *Phys. Rev. D* **8** (1973) 3633–3652.
34. H. D. Politzer, *Phys. Rept.* **14** (1974) 129–180.
35. S. Bethke, *Nucl. Phys. B* (*Proc. Suppl.*) **222–224** (2012) 94–100.
36. B. Schenke, C. Gale and S. Jeon, *Phys. Rev. C* **80** (2009) 054913.
37. P. Tribedy and R. Venugopalan, *Phys. Lett. B* **710** (2012) 125–133.
38. D. J. Gross, R. D. Pisarski and L. G. Yaffe, *Rev. Mod. Phys.* **53** (1981) 43.
39. J. O. Andersen, M. Strickland and N. Su, *JHEP* **1008** (2010) 113.
40. J. O. Andersen, L. E. Leganger, M. Strickland and N. Su, *JHEP* **1108** (2011) 053.
41. N. Haque, M. G. Mustafa and M. Strickland, *Phys. Rev. D* **87**(10) (2013) 105007.
42. A. Ali Khan *et al.*, *Phys. Rev. D* **64** (2001) 074510.
43. M. Cheng, S. Ejiri, P. Hegde, F. Karsch, O. Kaczmarek *et al.*, *Phys. Rev. D* **81** (2010) 054504.
44. S. Borsanyi, Z. Fodor, C. Hoelbling, S. D. Katz, S. Krieg *et al.*, *Phys. Lett. B* **730** (2014) 99–104.
45. H. B. Meyer, *Phys. Rev. Lett.* **100** (2008) 162001.
46. H. B. Meyer, *Phys. Rev. D* **76** (2007) 101701.
47. J. Noronha-Hostler, J. Noronha and C. Greiner, *Phys. Rev. Lett.* **103** (2009) 172302.
48. D. Fernandez-Fraile and A. Gomez Nicola, *Eur. Phys. J. C* **62** (2009) 37–54.
49. A. Buchel, *Phys. Lett. B* **663** (2008) 286–289.
50. S. S. Gubser, S. S. Pufu and F. D. Rocha, *JHEP* **0808** (2008) 085.
51. T. Springer, C. Gale and S. Jeon, *Phys. Rev. D* **82** (2010) 126011.
52. P. B. Arnold, G. D. Moore and L. G. Yaffe, *JHEP* **0301** (2003) 030.
53. S. Dubovsky, L. Hui, A. Nicolis and D. T. Son, *Phys. Rev. D* **85** (2012) 085029.
54. P. Danielewicz and M. Gyulassy, *Phys. Rev. D* **31** (1985) 53–62.
55. G. Policastro, D. T. Son and A. O. Starinets, *Phys. Rev. Lett.* **87** (2001) 081601.
56. P. Romatschke and U. Romatschke, *Phys. Rev. Lett.* **99** (2007) 172301.
57. H. Song, S. A. Bass, U. Heinz, T. Hirano and C. Shen, *Phys. Rev. Lett.* **106** (2011) 192301.
58. C. Gale, S. Jeon, B. Schenke, P. Tribedy and R. Venugopalan, *Phys. Rev. Lett.* **110** (2013) 012302.
59. U. Heinz and R. Snellings, *Ann. Rev. Nucl. Part. Sci.* **63** (2013) 123–151.
60. G. Denicol, H. Niemi, E. Molnar and D. Rischke, *Phys. Rev. D* **85** (2012) 114047.
61. H. Song and U. W. Heinz, *Phys. Rev. C* **81** (2010) 024905.
62. B. Betz, D. Henkel and D. Rischke, *J. Phys. G* **36** (2009) 064029.

63. G. Denicol, S. Jeon and C. Gale, *Phys. Rev. C* **90**(2) (2014) 024912.
64. W. Hiscock and L. Lindblom, *Annals Phys.* **151** (1983) 466–496.
65. W. A. Hiscock and L. Lindblom, *Phys. Rev. D* **31** (1985) 725–733.
66. H. Song and U. W. Heinz, *Phys. Rev. C* **78** (2008) 024902.
67. U. Heinz, H. Song and A. K. Chaudhuri, *Phys. Rev. C* **73** (2006) 034904.
68. E. Molnár, H. Niemi, G. Denicol and D. Rischke, *Phys. Rev. D* **89** (2014) 074010.
69. M. A. York and G. D. Moore, *Phys. Rev. D* **79** (2009) 054011.
70. G. D. Moore and K. A. Sohrabi, *JHEP* **1211** (2012) 148.
71. S. I. Finazzo, R. Rougemont, H. Marrochio and J. Noronha, Hydrodynamic transport coefficients for the non-conformal quark–gluon plasma from holography. (2014).
72. G. S. Denicol, W. Florkowski, R. Ryblewski and M. Strickland, *Phys. Rev. C* **90** (2014) 044905.
73. M. Martinez and M. Strickland, *Nucl. Phys. A* **848** (2010) 183–197.
74. W. Florkowski and R. Ryblewski, *Phys. Rev. C* **83** (2011) 034907.
75. P. Romatschke and M. Strickland, *Phys. Rev. D* **68** (2003) 036004.
76. M. Martinez, R. Ryblewski and M. Strickland, *Phys. Rev. C* **85** (2012) 064913.
77. D. Bazow, U. W. Heinz and M. Strickland, *Phys. Rev. C* **90**(5) (2014) 054910.
78. G. Baym, *Phys. Lett. B* **138** (1984) 18–22.
79. W. Florkowski, R. Ryblewski and M. Strickland, *Nucl. Phys. A* **916** (2013) 249–259.
80. W. Florkowski, R. Ryblewski and M. Strickland, *Phys. Rev. C* **88** (2013) 024903.
81. W. Florkowski, E. Maksymiuk, R. Ryblewski and M. Strickland, *Phys. Rev. C* **89**(5) (2014) 054908.
82. W. Florkowski, R. Ryblewski, M. Strickland and L. Tinti, *Phys. Rev. C* **89** (2014) 054909.
83. G. S. Denicol, U. W. Heinz, M. Martinez, J. Noronha and M. Strickland, *Phys. Rev. Lett.* **113** (2014) 202301.
84. G. S. Denicol, U. W. Heinz, M. Martinez, J. Noronha and M. Strickland, *Phys. Rev. D* **90** (2014) 125026.
85. S. S. Gubser, *Phys. Rev. D* **82** (2010) 085027.
86. S. S. Gubser and A. Yarom, *Nucl. Phys. B* **846** (2011) 469–511.
87. M. Nopoush, R. Ryblewski and M. Strickland, Anisotropic hydrodynamics for conformal Gubser flow, *Phys. Rev. D* **91** (2015) 045007 [arXiv:1410.6790 [nucl.th]].
88. A. Jaiswal, *Phys. Rev. C* **88** (2013) 021903.
89. D. Bazow, U. Heinz and M. Martinez, *in preparation.* (2015).
90. J. Bjorken, *Phys. Rev. D* **27** (1983) 140–151.
91. P. F. Kolb, J. Sollfrank and U. W. Heinz, *Phys. Rev. C* **62** (2000) 054909.
92. B. Schenke, S. Jeon and C. Gale, *Phys. Rev. C* **82** (2010) 014903.
93. A. Muronga, *Phys. Rev. C* **69** (2004) 034903.
94. H. Nessyahu and E. Tadmor, *J. Comput. Phys.* **87** (1990) 408–463.
95. V. Schneider, U. Katscher, D. Rischke, B. Waldhauser, J. Maruhn *et al.*, *J. Comput. Phys.* **105** (1993) 92–107.
96. J. Sollfrank, P. Huovinen, M. Kataja, P. Ruuskanen, M. Prakash *et al.*, *Phys. Rev. C* **55** (1997) 392–410.
97. H. Petersen, G.-Y. Qin, S. A. Bass and B. Muller, *Phys. Rev. C* **82** (2010) 041901.
98. I. Karpenko and Y. Sinyukov, *Phys. Rev. C* **81** (2010) 054903.
99. H. Holopainen, H. Niemi and K. J. Eskola, *Phys. Rev. C* **83** (2011) 034901.
100. L. Pang, Q. Wang and X.-N. Wang, *Phys. Rev. C* **86** (2012) 024911.
101. V. Roy and A. Chaudhuri, *Phys. Rev. C* **85** (2012) 024909.
102. Y. Akamatsu, S.-I. Inutsuka, C. Nonaka and M. Takamoto, *J. Comput. Phys.* **256** (2014) 34–54.

103. A. Kurganov and E. Tadmor, *J. Comput. Phys.* **160** (2000) 241–282.
104. C. Shen, Z. Qiu, H. Song, J. Bernhard, S. Bass *et al.*, The iEBE-VISHNU code package for relativistic heavy-ion collisions. (2014).
105. T. Hirano and Y. Nara, *PTEP* **2012** (2012) 01A203.
106. C. Nonaka, N. Sasaki, S. Muroya and O. Miyamura, *Nucl. Phys. A* **661** (1999) 353–356.
107. L. Del Zanna, V. Chandra, G. Inghirami, V. Rolando, A. Beraudo *et al.*, *Eur. Phys. J. C* **73** (2013) 2524.
108. C. Aguiar, T. Kodama, T. Osada and Y. Hama, *J. Phys. G* **27** (2001) 75–94.
109. M. Luzum and P. Romatschke, *Phys. Rev. C* **78** (2008) 034915.
110. P. Bozek, *Phys. Rev. C* **85** (2012) 034901.
111. U. W. Heinz and P. F. Kolb, *Phys. Lett. B* **542** (2002) 216–222.
112. H. Song, S. A. Bass and U. Heinz, *Phys. Rev. C* **83** (2011) 024912.
113. H. Holopainen and P. Huovinen, *J. Phys. Conf. Ser.* **389** (2012) 012018.
114. F. Cooper and G. Frye, *Phys. Rev. D* **10** (1974) 186.
115. P. Huovinen and H. Petersen, *Eur. Phys. J. A* **48** (2012) 171.
116. F. Grassi, *Braz. J. Phys.* **35** (2005) 52–69.
117. Y. Sinyukov, S. Akkelin, I. Karpenko and Y. Hama, *Acta Phys. Polon. B* **40** (2009) 1025–1036.
118. D. Oliinychenko, P. Huovinen and H. Petersen, Systematic Investigation of Negative Cooper-Frye Contributions in Heavy Ion Collisions Using Coarse-grained Molecular Dynamics, *Phys. Rev. C* **91** (2015) 024906 [arXiv:1411.3912 [nucl-th]].
119. K. Dusling, G. D. Moore and D. Teaney, *Phys. Rev. C* **81** (2010) 034907.
120. G. Denicol and H. Niemi, *Nucl. Phys. A* **904–905** (2013) 369c–372c.
121. J. Noronha-Hostler, G. S. Denicol, J. Noronha, R. P. G. Andrade and F. Grassi, *Phys. Rev. C* **88** (2013) 044916.
122. J. Kapusta, B. Muller and M. Stephanov, *Phys. Rev. C* **85** (2012) 054906.
123. K. Murase and T. Hirano, Relativistic fluctuating hydrodynamics with memory functions and colored noises (2013).
124. T. Hirano, R. Kurita, K. Murase and K. Nagai, *Nucl. Phys. A* (2014).
125. C. Young, J. Kapusta, C. Gale, S. Jeon and B. Schenke, *J. Phys. Conf. Ser.* **535** (2014) 012034.
126. C. Young, J. Kapusta, C. Gale, S. Jeon and B. Schenke, Thermally Fluctuating Second-Order Viscous Hydrodynamics and Heavy-Ion Collisions, *Phys. Rev. C* **91** (2015) 044901 [arXiv:1407.1077 [nucl-th]].